

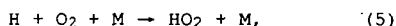
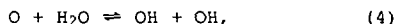
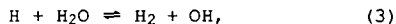
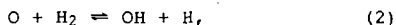
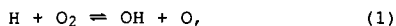
THERMAL RATE CONSTANT MEASUREMENTS BY THE
FLASH OR LASER PHOTOLYSIS-SHOCK TUBE METHOD:
RESULTS FOR THE OXIDATIONS OF H₂ AND D₂

J. V. Michael
Chemistry Division
Argonne National Laboratory
Argonne, IL 60439

Keywords: Rate constants, Shock tubes, H₂ and D₂ oxidations

INTRODUCTION

This article discusses the FP- or LP-ST technique. The modeling of the oxidation of H₂ will be specifically featured. The reactions that pertain to this oxidative system and that have been studied by either the FP- or LP-ST technique, will be reviewed. These include,



and their deuterated modifications. Both forward and reverse processes will be included in the discussion since, in all cases, the existing data indicate that the reactions are microscopically reversible. Hence, data evaluations can be made over very large temperature ranges.

EXPERIMENTAL

The FP-ST technique was first suggested by Burns and Hornig¹ and was followed by some OH-radical reaction studies by Zellner and coworkers.² The technique has recently been extended with the atomic resonance absorption spectroscopic (ARAS) method of detection.³ This extension naturally follows from the earlier work.^{1,2} A less ambiguous experiment is now possible since spectroscopic absorption by atomic species is stronger than by diatomic or polyatomic radicals, and thus, smaller concentrations can be detected thereby eliminating complications from secondary reactions. This development has allowed absolute bimolecular rate constants to be directly studied over a large T-range, ~650 to 2500 K.

The shock tube methods that are used in FP- or LP-ST studies are traditional.⁴ A schematic diagram of a recently constructed apparatus⁵ is shown in Fig. 1. The technique has been described previously,^{5,6,7} and therefore, only a brief description will be given here. The method utilizes the double heating effect that can be obtained by reflected shock wave methods. The nearly stagnant gas in the reflected shock wave regime is subjected to either flash or laser photolysis thereby producing an atomic species in the central hot gas region. The time dependence of the atomic species is then radially monitored as it reacts with an added reactant molecule. It is

necessary to have a source molecule present which, on photolysis, gives the atomic species of interest.

If the transmittance for any atomic absorption experiment can be held above ~0.8, then Beer's law will hold to a good approximation if the line is not too highly reversed. In FP- and LP-ST experiments with unreversed or only partially reversed resonance lamps, it is therefore only necessary to measure the temporal behavior of absorbance, (ABS), where $(ABS) \equiv -\ln(I/I_0)$. Since Beer's law holds, the atom concentration, [A], is equal to $(ABS)/\sigma_A l$. In all cases, the reactant concentration is very much larger than that of the atom, and therefore, the decay of A will obey pseudo-first-order kinetics. Since [A] is proportional to (ABS), it is only necessary to measure the temporal behavior of absorbance, $(ABS)_t$, in a kinetics experiment. The rate of depletion of the atomic species is the product of the thermal rate constant times the concentrations of the reactant and the depleting atomic concentration. After integration, a plot of $\ln(ABS)_t$ against time will yield a decay constant that is equal to the product of the thermal rate constant times the reactant concentration. Fig. 2 shows a typical plot of an experiment. The top panel shows an actual raw data signal and the bottom panel shows the first-order plot derived from the top panel. The negative slope of the plot gives the decay constant which, on division by the reactant concentration, gives a measurement of the thermal rate constant at the conditions of the experiment as determined from the initial pressure, temperature, and the shock strength.

RESULTS

$H + O_2 \rightarrow OH + O$ and $D + O_2 \rightarrow OD + O$: The first published LP-ST paper⁸ showed that the photolysis of H_2O at 193 nm yields both H-atoms and OH-radicals at high temperatures. In recent LP-ST experiments,⁹ H_2O photolyte was used at $T \approx 1085$ K. With the higher fluences from excimer laser photolysis, experiments could be performed with less H_2O being present than in an earlier FP-ST study that used the same technique of detection.¹⁰ This has allowed experiments to be performed at substantially higher T, up to 2278 K. Fig. 2 shows a typical experiment. Data with both H_2O and NH_3 as photolyte molecules have yielded the Arrhenius result,

$$k_1 = (1.15 \pm 0.16) \times 10^{-10} \exp(-6917 \pm 193 \text{ K/T}) \text{ cm}^3 \text{ molecule}^{-1} \text{ s}^{-1}, \quad (6)$$

for $1103 \leq T \leq 2055$ K. Similar results for reaction (1D) with D_2O as photolyte give the Arrhenius result,

$$k_{1D} = (1.09 \pm 0.20) \times 10^{-10} \exp(-6937 \pm 247 \text{ K/T}) \text{ cm}^3 \text{ molecule}^{-1} \text{ s}^{-1}, \quad (7)$$

for $1085 \leq T \leq 2278$ K. The reverse rate constants can be determined from JANAF equilibrium values,¹¹ and rate constants for forward and reverse processes are listed in Table I.

$O + H_2 \rightarrow OH + H$ and $O + D_2 \rightarrow OD + H$: FP-ST experiments with NO as the O-atom source have been carried out on both the H_2 ¹² and D_2 ⁵ reactions. The results for $O + H_2$ can be described by the Arrhenius equation,

$$k_2 = (3.10 \pm 0.20) \times 10^{-10} \exp(-6854 \pm 84 \text{ K/T}) \text{ cm}^3 \text{ molecule}^{-1} \text{ s}^{-1}, \quad (8)$$

for $880 \leq T \leq 2495$ K. $O + D_2$ can similarly be described by,

$$k_{2D} = (3.22 \pm 0.25) \times 10^{-10} \exp(-7293 \pm 98 \text{ K/T}) \text{ cm}^3 \text{ molecule}^{-1} \text{ s}^{-1}, \quad (9)$$

for $825 \leq T \leq 2487$ K. Earlier shock tube determinations are in reasonable agreement with these direct results. There are also a number of lower temperature determinations for k_2 ¹²⁻¹⁶ and k_{2D} ¹⁴⁻¹⁸. The most reliable low T data are those of Sutherland et al.,¹² Westenberg and deHaas,^{13,17} Presser and Gordon,¹⁶ and Zhu et al.¹⁸ These data have been combined with the FP-ST data to give three parameter expressions that can be used over the entire experimental temperature range.

$$k_2 = 8.44 \times 10^{-20} T^{2.67} \exp(-3167 \text{ K/T}) \text{ cm}^3 \text{ molecule}^{-1} \text{ s}^{-1}, \quad (10)$$

for $297 \leq T \leq 2495$ K,¹² and,

$$k_{2D} = 2.43 \times 10^{-16} T^{1.70} \exp(-4911 \text{ K/T}) \text{ cm}^3 \text{ molecule}^{-1} \text{ s}^{-1}, \quad (11)$$

for $343 \leq T \leq 2487$ K.⁵ Eqs. (10) and (11) agree within a few percent with all studies except that of Marshall and Fontijn.¹⁵ Rate constants for the reverse reactions can be calculated from JANAF equilibrium constant values,¹¹ and the values for both forward and reverse rate constants are compiled in Table I.

$H + H_2O \rightarrow H_2 + OH$ and $D + D_2O \rightarrow D_2 + OD$: There are only two direct studies of reaction (3), one being with the FP-ST¹⁹ and the other being with the LP-ST⁸ techniques. The results from these two studies are given in Arrhenius form as,

$$k_3 = (4.58 \pm 0.61) \times 10^{-10} \exp(-11558 \pm 243 \text{ K/T}) \text{ cm}^3 \text{ molecule}^{-1} \text{ s}^{-1}, \quad (12)$$

for $1246 \leq T \leq 2297$ K, and,

$$k_3 = (3.99 \pm 0.42) \times 10^{-10} \exp(-10750 \pm 500 \text{ K/T}) \text{ cm}^3 \text{ molecule}^{-1} \text{ s}^{-1}, \quad (13)$$

for $1600 \leq T \leq 2500$ K, respectively. These two equations agree within combined error limits over the range of T overlap. At high T, there is only one direct FP-ST study²⁰ of reaction (3D). These results are described for $1285 \leq T \leq 2261$ K by the Arrhenius expression.

$$k_{3D} = (2.90 \pm 0.73) \times 10^{-10} \exp(-10815 \pm 356 \text{ K/T}) \text{ cm}^3 \text{ molecule}^{-1} \text{ s}^{-1} \quad (14)$$

There are numerous earlier studies²¹⁻²⁵ of reaction (-3) with four being particularly notable.^{21,23-25} JANAF equilibrium constants¹¹ have been used to transform these reverse rate constant data²⁵ to those for the forward process, and an evaluation has been carried out for $250 \leq T \leq 2581$ K. A three parameter expression describes the results.

$$k_3 = 1.56 \times 10^{-15} T^{1.52} \exp(-9249 \text{ K/T}) \text{ cm}^3 \text{ molecule}^{-1} \text{ s}^{-1}. \quad (15)$$

Since the data are not as extensive, an extended expression for k_{3D} cannot be evaluated; however, values for the back reaction (-3D) can be derived from JANAF values.¹¹ This expression and the other derived expressions are given in Table I.

$O + H_2O \rightarrow OH + OH$ and theory for $O + D_2O \rightarrow OD + OD$: There are three direct studies of reaction (4)²⁶⁻²⁸ for the T-ranges, 1053-2033 K,²⁶ 1500-2500 K,²⁷ and 753-1045 K,²⁸ respectively. The FP-ST results from Sutherland, et al.²⁶ can be represented by the Arrhenius equation,

$$k_4 = 1.10 \times 10^{-10} \exp(-9929 \text{ K/T}) \text{ cm}^3 \text{ molecule}^{-1} \text{ s}^{-1}, \quad (16)$$

for $1288 \leq T \leq 2033$ K. The results from Lifshitz and Michael²⁷ are,

$$k_4 = (1.12 \pm 0.20) \times 10^{-10} \exp(-9115 \pm 304 \text{ K/T}) \text{ cm}^3 \text{ molecule}^{-1} \text{ s}^{-1}, \quad (17)$$

for $1500 \leq T \leq 2500$ K. The activation energies are different with the latter being lower than the former by ~10%. Evenso, the agreement between the two studies is good with eq. (16) being ~30-40% lower than that of eq. (17). The spread in the data from each study is ~±15-20%, and the two sets overlap over the common T-range. Sutherland, et al.²⁶ have also carried out Flash Photolysis-Resonance Fluorescence (FP-RF) studies at lower T, 1053 to 1123 K, and these data are the most accurate to date for reaction (4). There are numerous experimental studies of the back reaction (-4).^{22b,29} These data have been combined with that from the two FP-ST studies through the JANAF equilibrium constants¹¹, and a comparison between the combined database for reactions (4) and (-4) with theoretical calculations has been made.⁷ The theoretical result,

$$k_4^{\text{th}} = 7.48 \times 10^{-20} T^{2.70} \exp(-7323 \text{ K/T}) \text{ cm}^3 \text{ molecule}^{-1} \text{ s}^{-1}, \quad (18)$$

agrees with experiment within experimental error over the T-range, 700-2500 K. There are no data for the $O + D_2O$ reaction. Therefore, a theoretical estimate that is consistent with the successful protonated case, eq. (18),⁷ can be used as a starting point in experiment design and/or in chemical modeling experiments for the D_2/O_2 system. The calculated result for $700 \leq T \leq 2500$ K is,

$$k_{4D}^{\text{th}} = 2.05 \times 10^{-19} T^{2.56} \exp(-8286 \text{ K/T}) \text{ cm}^3 \text{ molecule}^{-1} \text{ s}^{-1}. \quad (19)$$

These expressions and the transformed reverse rate constant values are listed in Table I.

$H + O_2 + M \rightarrow HO_2 + M$: FP-ST results have been obtained for this reaction.¹⁰ The third-order rate constant has been determined for $746 \leq T \leq 987$ K to be $k_5 = (7.1 \pm 1.9) \times 10^{-33} \text{ cm}^6 \text{ molecule}^{-2} \text{ s}^{-1}$ with Ar as the heat bath gas.¹⁰ The Baulch et al.³⁰ recommendation is,

$$k_{H+O_2+Ar} = 4.1 \times 10^{-33} \exp(+500 \text{ K/T}) \text{ cm}^6 \text{ molecule}^{-2} \text{ s}^{-1}. \quad (20)$$

A recent flow tube study³¹ for $298 \leq T \leq 639$ K in He gives,

$$k_{H+O_2+He} = (4.0 \pm 1.2) \times 10^{-33} \exp(+560 \text{ K/T}) \text{ cm}^6 \text{ molecule}^{-2} \text{ s}^{-1}. \quad (21)$$

Since He and Ar have about the same effective collision efficiency, the FP-ST result can be compared to both eqs. (20) and (21). At the mean temperature, $T = 850$ K, eqs. (20) and (21) give respective values of 7.4×10^{-33} and 7.7×10^{-33} to be compared to the FP-ST result of $7.1 \times 10^{-33} \text{ cm}^6 \text{ molecule}^{-2} \text{ s}^{-1}$. These results combine to give excellent agreement for the recombination reaction over the

temperature range, 300 to ~1000 K. Since the Hsu et al.³¹ result is the most direct to date, it is listed in Table I. Similar experiments for $D + O_2 + M$ have not been reported, but eq. (21) can be used in D_2/O_2 modeling calculations as a first estimate.

CONCLUSION

The most important rate constants in the branching chain oxidations of H_2 and D_2 have now been measured by the direct flash and/or laser photolysis-shock (FP- or LP-ST) tube technique. The only exceptions are the $O + D_2O$ and $D + O_2 + M$ reactions. There are of course several other reactions of secondary importance that must be included in complete oxidation mechanisms, and these have been considered in most earlier studies. The importance of these reactions increases as the extent of reaction increases, and, in the large conversion H_2/O_2 studies where OH-radicals are observed throughout the entire course of the reaction, the relative effects of these secondary reactions are greater than in the small conversion studies where the initial stages of the reaction are only monitored. However, even in the high conversion studies, the five reactions considered here and their reverses, always exhibit higher sensitivity than all other reactions in sensitivity analysis calculations. It can therefore be concluded with these new direct FP- and LP-ST data that the main features of the oxidation mechanisms are now substantially solved.

The evaluated rate constants are given in Table I along with comments regarding accuracy and the T-range of applicability. We recommend that these rate constants be used as initial starting values in oxidation studies. To be sure, the rate constants are known only within certain error limits, and therefore, any adjustments within these error limits are certainly allowed. However, if a particular observation implies the use of rate constants that are substantially outside the bounds set by these direct studies, then an inconsistency exists. In this event, new explanations must be found, and this may imply modifications in the reaction rate constants for initiation and/or perhaps in secondary chemical processes.

ACKNOWLEDGEMENT

This work was supported by the U. S. Department of Energy, Office of Basic Energy Sciences, Division of Chemical Sciences, under Contract No. W-31-109-Eng-38.

REFERENCES

1. Burns, G. and Hornig, D.F., *Can. J. Chem.* **38**, 1702 (1960).
2. (a) Ernst, J., Wagner, H. G. and Zellner, R., *Ber. Bunsen-Ges. Phys. Chem.* **82**, 409 (1978). (b) Niemitz, K. J., Wagner, H. G. and Zellner, R., *Z. Phys. Chem. (Frankfurt am Main)* **124**, 155 (1981).
3. Michael, J. V., Sutherland, J. W. and Klemm, R. B., *Int. J. Chem. Kin.* **17**, 315 (1985).
4. Bradley, J. N., *Shock Waves in Chemistry and Physics*, Wiley, New York, 1962.
5. Michael, J. V., *J. Chem. Phys.* **90**, 189 (1989).
6. Michael, J. V., *Adv. Chem. Kin. and Dynamics* **1**, xxx (1991).
7. Michael, J. V., *Prog. Energy and Combust. Sci.*, submitted.
8. Davidson, D. F., Chang, A. Y. and Hanson, R. K., *Symp. (Int.) Combust., [Proc.]* **22**, 1877 (1988).

9. Shin, K. S. and Michael, J. V., *J. Chem. Phys.*, in press.
10. Pirraglia, A. N., Michael, J. V., Sutherland, J. W. and Klemm, R. B., *J. Phys. Chem.* **93**, 282 (1989).
11. Chase, Jr., M. W., Curnutt, J. L., Downey, Jr., J. R., McDonald, R. A., Syverud, A. N. and Valenzuela, E. A., *J. Phys. Chem. Ref. Data* **15**, 1078 (1986).
12. Sutherland, J. W., Michael, J. V., Pirraglia, A. N., Nesbitt, F. L. and Klemm, R. B., *Symp. (Int.) Combust.*, [Proc.] **21**, 929 (1986).
13. Westenberg, A. A. and deHaas, N., *J. Chem. Phys.* **46**, 490 (1967); *ibid* **50**, 2512 (1969).
14. Clyne, M. A. A. and Thrush, B. A., *Proc. R. Soc. London Ser. A* **275**, 544 (1963).
15. Marshall, P. and Fontijn, A., *J. Chem. Phys.* **87**, 6988 (1987).
16. Presser, N. and Gordon, R. J., *J. Chem. Phys.* **82**, 1291 (1985).
17. Westenberg, A. A. and de Haas, N., *J. Chem. Phys.* **47**, 4241 (1967).
18. Zhu, Y.-F., Arepalli, S. and Gordon, R. J., *J. Chem. Phys.* **90**, 183 (1989).
19. Michael, J. V. and Sutherland, J. W., *J. Phys. Chem.* **92**, 3853 (1988).
20. Fisher, J. R. and Michael, J. V., *J. Phys. Chem.* **94**, 2465 (1990).
21. Frank P. and Just, Th., *Ber. Bunsen-Ges. Phys. Chem.* **89**, 181 (1985). 2
22. (a) Kaufman, F. and delGreco, F.P., *Discuss. Faraday Soc.* **33**, 128 (1962); (b) Dixon-Lewis, G., Wilson, W. E. and Westenberg, A. A., *J. Chem. Phys.* **44**, 2877 (1966); (c) Greiner, N. R., *J. Chem. Phys.* **51**, 5049 (1969); (d) Stuhl, F. and Niki, H., *J. Chem. Phys.* **57**, 3671 (1972); (e) Westenberg, A. A. and deHaas, N., *J. Chem. Phys.* **58**, 4061 (1973); (f) Smith, I. W. M. and Zellner, R., *J. Chem. Soc., Faraday Trans. 2* **70**, 1045 (1974); (g) Atkinson, R., Hansen, D. A. and Pitts, Jr., J. N., *J. Chem. Phys.* **63**, 1703 (1975); (h) Overend, R. P., Paraskevopoulos, G. and Cvetanovic, R. J., *Can. J. Chem.* **53**, 3374 (1975).
23. Ravishankara, A. R., Nicovich, J. M., Thompson, R. L. and Tully, F. P., *J. Phys. Chem.* **85**, 2498 (1981).
24. Tully, F. P. and Ravishankara, A. R., *J. Phys. Chem.* **84**, 3126 (1980).
25. Oldenborg, R. C., Harradine, D. M., Loge, G. W. and Winn, K. R., Paper presented at the Second International Conference on Chemical Kinetics, N. I. S. T., Gaithersburg, MD, July 24, 1989.
26. Sutherland, J. W., Patterson, P. M. and Klemm, R. B., *Symp. (Int.) Combust.*, [Proc.] **23**, xxx (1990).
27. Lifshitz, A. and Michael, J. V., *Symp. (Int.) Combust.*, [Proc.] **23**, xxx (1990).
28. Albers, E. A., Hoyermann, K., Wagner, H. Gg. and Wolfrum, J., *Symp. (Int.) Combust.*, [Proc.] **13**, 81 (1970).
29. (a) Rawlins, W. T. and Gardiner, Jr., W. C., *J. Chem. Phys.* **60**, 4676 (1974); (b) Ernst, J., Wagner, H. Gg. and Zellner, R., *Ber. Bunsenges. Phys. Chem.* **81**, 1270 (1977); (c) del Greco, F. P. and Kaufman, F., *Disc. Faraday Soc.* **33**, 128 (1962) and Kaufman, F., *Ann. Geophys.* **20**, 106 (1964); (d) Wilson, W. E. and O'Donovan, J. T., *J. Chem. Phys.* **47**, 5455 (1967); (e) Breen, J. E. and Glass, G. P., *J. Chem. Phys.* **52**, 1082 (1970); (f) Westenberg, A. A. and de Haas, N., *J. Chem. Phys.* **58**, 4066 (1973); (g) McKenzie, A., Mulcahy, M. F. R. and Steven, J. P., *J. Chem. Phys.* **59**, 3244 (1973); (h) Clyne, M. A. A. and Down, S., *J. Chem. Soc. Faraday Trans. II* **70**, 253 (1974); (i) Trainor, D. W.

- and von Rosenberg, C. W., Jr., *J. Chem. Phys.* **61**, 1010 (1974);
 (j) Farquharson, G. K. and Smith, R. H., *Aust. J. Chem.* **33**, 1425
 (1980); (k) Wagner, G. and Zellner, R., *Ber. Bunsenges. Phys.*
Chem. **85**, 1122 (1981).
30. Baulch, D. L., Drysdale, D. D., Horne, D. G. and Lloyd, A. C.,
 vol. 1 of *Evaluated Data for High Temperature Reactions*,
 Butterworths, London, 1972.
31. Hsu, K.-J., Durant, J. L. and Kaufman, F., *J. Phys. Chem.* **91**,
 1985 (1987); Hsu, K.-J., Anderson, S. M., Durant, J. L. and
 Kaufman, F., *J. Phys. Chem.* **93**, 1018 (1989).

Table I: Recommended $k = A T^n \exp(-B/T)$ expressions for the H_2/O_2 and D_2/O_2 Reactions from the FP- or LP-ST Studies.

| Reaction | $A/cm^3 \text{ molecule}^{-1} \text{ s}^{-1}$ | n | B/K | Comments and Reference |
|-----------------------|---|------|--------|--|
| Protonated reactions: | | | | |
| $H + O_2$ | $1.15(-10)^a$ | 0 | -6917 | 1100 - 2050K, $\pm 27\%$ ⁹ |
| $OH + O$ | $8.75(-12)$ | 0 | 1121 | 1100 - 2050K, $\pm 27\%$ ^{9,11} |
| $O + H_2$ | $8.44(-20)$ | 2.67 | -3167 | 297 - 2495K, $\pm 30\%$ ¹² |
| $OH + H$ | $3.78(-20)$ | 2.67 | -2226 | 297 - 2495K, $\pm 30\%$ ^{11,12} |
| $H + H_2O$ | $1.56(-15)$ | 1.52 | -9249 | 250 - 2297K, $\sim \pm 25\%$ ^{11,25} |
| $OH + H_2$ | $3.56(-16)$ | 1.52 | -7513 | 250 - 2581K, $\sim \pm 25\%$ ²⁵ |
| $O + H_2O$ | $7.48(-20)$ | 2.70 | -7323 | 700 - 2500K, $\sim \pm 50\%$, theory ⁷ |
| $OH + OH$ | $7.19(-21)$ | 2.70 | 1251 | 700 - 2500K, $\sim \pm 50\%$, theory ⁷ |
| $H + O_2 + M$ | $4.0(-33)^b$ | 0 | 560 | 298 - $\sim 1000K$, $\sim \pm 30\%$ ³¹ |
| Deuterated reactions: | | | | |
| $D + O_2$ | $1.09(-10)$ | 0 | -6937 | $1050 \leq T \leq 2300K$, $\pm 27\%$ ⁹ |
| $OD + O$ | $9.73(-12)$ | 0 | 526 | $1050 \leq T \leq 2300K$, $\pm 27\%$ ^{9,11} |
| $O + D_2$ | $2.43(-16)$ | 1.70 | -4911 | $343 \leq T \leq 2487K$, $\pm 16\%$ ⁵ |
| $OD + D$ | $1.04(-16)$ | 1.70 | -3806 | $343 \leq T \leq 2487K$, $\pm 16\%$ ^{5,11} |
| $D + D_2O$ | $2.90(-10)$ | 0 | -10815 | $1285 \leq T \leq 2261K$, $\pm 27\%$ ²⁰ |
| $OD + D_2$ | $6.56(-11)$ | 0 | -3320 | $1285 \leq T \leq 2261K$, $\pm 27\%$ ^{11,20} |
| $O + D_2O$ | $2.05(-19)$ | 2.56 | -8286 | $> 700 K$, theory ⁷ |
| $OD + OD$ | $1.85(-20)$ | 2.56 | 452 | $> 700 K$, theory ⁷ |

^aparentheses denotes the power of ten; i. e., 1.15×10^{-10} . ^bunits are $\text{cm}^6 \text{ molecule}^{-2} \text{ s}^{-1}$.

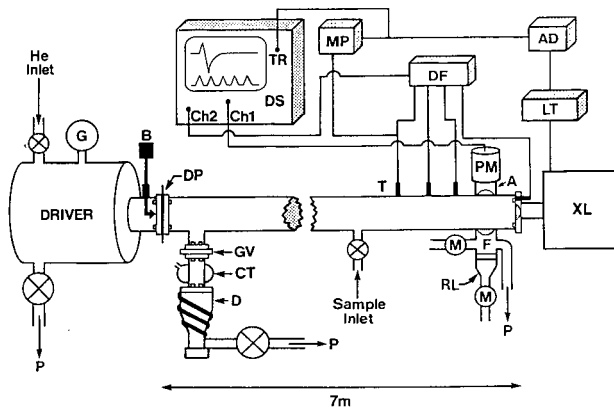


Fig. 1: Schematic diagram of the apparatus. P - rotary pump. D - oil diffusion pump. CT - liquid nitrogen baffle. GV - gate valve. G - bourdon gauge. B - breaker. DP - diaphragm. T - pressure transducers. M - microwave power supply. F - atomic filter. RL - resonance lamp. A - gas and crystal window filter. PM - photomultiplier. DS - digital oscilloscope. MP - master pulse generator. TR - trigger pulse. DF - differentiator. AD - delayed pulse generator. LT - laser trigger. XL - excimer laser.

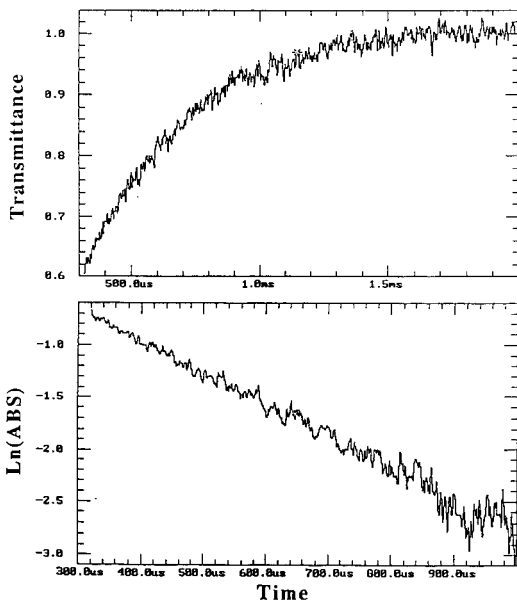


Fig. 2: Top: H-atom transmittance as a function of time after laser photolysis in the reflected shock wave region. Bottom: First-order plot of $\ln[\text{ABS}]_t$ against time that is obtained from the top record.

PHOTOIONIZATION MASS SPECTROMETRIC STUDIES OF THE COMBUSTION
INTERMEDIATES CH₂OH AND CH₃O*

B. Ruscic and J. Berkowitz
Chemistry Division
Argonne National Laboratory
Argonne, IL 60439

I. INTRODUCTION

The radical species CH₃O and CH₂OH are believed to play important roles as intermediates in the combustion of hydrocarbon fuels.^{1,2} Recently, absorption spectra in the visible-UV have been observed for both species,³⁻¹⁰ primarily using laser methods. Accurate experimental vibrational frequencies are known for both species, and a rotational analysis (and hence geometric structure) is known for CH₃O. Despite this intensive study, the heats of formation of these species are still somewhat uncertain.

Cruikshank and Benson¹¹ studied the iodination reaction



and obtained an endothermicity of 24.6 ± 1.5 kcal/mol. Utilizing this value, Golden and Benson¹² compute $\Delta H^\circ_{f,298}(\text{CH}_2\text{OH}) = -4.2 \pm 1.5$ kcal/mol. However, Golden and Benson also cite Buckley and Whittle,¹³ who studied the corresponding bromination reaction, and inferred an endothermicity of < 4.2 kcal/mol. From this latter observation, one can deduce $\Delta H^\circ_{f,298}(\text{CH}_2\text{OH}) \leq -8.3$ kcal/mol. In order to give some weight to the bromination data, Golden and Benson¹² chose $\Delta H^\circ_{f,298}(\text{CH}_2\text{OH}) = -6.2 \pm 2.5$ kcal/mol. The compilation of Glushko et al.¹⁴ selects $\Delta H^\circ_{f,298}(\text{CH}_2\text{OH}) = -4.8 \pm 2.4$ kcal/mol as the middle range of several experiments, three of which are based on an incorrect ionization potential of CH₂OH (vide infra).

For $\Delta H^\circ_f(\text{CH}_3\text{O})$, most recent papers cite the experiments of Batt and co-workers.¹⁵⁻¹⁷ Batt and Milne¹⁶ determined the bond energy of CH₃O-NO by kinetic measurements (assuming no reverse activation energy) to be 41.8 kcal/mol. Using $\Delta H^\circ_{f,298}(\text{CH}_3\text{ONO}) = -16.0$ kcal/mol from Silverwood and Thomas,¹⁸ they obtained $\Delta H^\circ_{f,298}(\text{CH}_3\text{O}) = 4.2 \pm 0.7$ kcal/mol. Subsequently, Batt and McCulloch¹⁷ obtained $\Delta H^\circ_{f,298}(\text{CH}_3\text{O}) = 3.8 \pm 0.2$ kcal/mol from the kinetics of dimethyl peroxide pyrolysis. Glushko, et al.,¹⁴ surprisingly not citing Batt and co-workers, arrive at 3.1 ± 1 kcal/mol from an examination of other sources.

At this point, it is convenient to introduce some *ab initio* calculations which have focused on the difference in stabilities of CH₂OH and CH₃O. Saebo et al.¹⁹ show that CH₃O is 4.1 kcal/mol more stable than CH₂OH at the Hartree-Fock level (6-31 G** basis sets). However, when electron correlation is included, CH₂OH becomes more stable. At the MP3/6-31 G** level, and including zero point energies, CH₂OH is 5.0 kcal/mol more stable than CH₃O. At this level, the barrier to isomerization (CH₃O \rightarrow CH₂OH) is found to be 36.0 kcal/mol. Later, Colwell²⁰ obtained an almost identical result - CH₂OH more stable by 5.86 kcal/mol, and a barrier height of 37.29 kcal/mol - using CI (singles and doubles) with a Davidson correction and a double zeta plus polarization basis set. However, in the recent calculation by Curtiss et al.²¹ at the G2 level (more correlation) CH₂OH is found to be 8.8 kcal/mol more stable than CH₃O. Our prior analysis of experimental data would lead to a difference of $(8.4 - 10.4) \pm 2$ kcal/mol. A previous experimental estimate of this quantity by Batt et al.²² arrived at 7.5 kcal/mol.

The adiabatic ionization potential (I.P.) of a molecular species is the difference between the heats of formation of that species and the corresponding cation. Hence, if the heat of formation of the desired

* Work supported by the U.S. Department of Energy, Office of Basic Energy Sciences, Division of Chemical Sciences, under Contract W-31-109-ENG-38.

cation is well known, and its adiabatic I.P. can be obtained, it offers an alternative route to the heat of formation of the neutral species. It turns out that $\Delta H_f^\circ(\text{CH}_2\text{OH}^+)$ is rather well known from photoionization measurements²³ of the appearance potential of CH_2OH^+ from CH_3OH and $\text{C}_2\text{H}_5\text{OH}$. These measurements yield $\Delta H_f^\circ(\text{CH}_2\text{OH}^+) \geq 172.0 \pm 0.7$ and ≤ 171.7 kcal/mol, respectively. The adiabatic ionization potential of CH_2OH has been obtained in a photoelectron spectroscopic study by Dyke and co-workers,²⁴ who obtained I.P. (CH_2OH) = 7.56 ± 0.01 eV. We shall re-examine this result in the experiments to be described below. Combining $\Delta H_f^\circ(\text{CH}_2\text{OH}^+)$ and I.P. (CH_2OH), we obtain $\Delta H_{f_0}^\circ(\text{CH}_2\text{OH}) \leq -2.3 \pm 0.7$ kcal/mol, or $\Delta H_{f_{298}}^\circ(\text{CH}_2\text{OH}) \leq -3.9 \pm 0.7$ kcal/mol.

In the case of CH_3O , the heat of formation of its cation is very much in question. Dyke²⁵ reports 7.37 ± 0.03 eV as the adiabatic I.P. of CH_3O . Taking $\Delta H_f^\circ(\text{CH}_3\text{O}) = 4.0 \pm 1$ kcal/mol (vide supra), we infer $\Delta H_f^\circ(\text{CH}_3\text{O}^+) = 174$ kcal/mol. (We ignore for the moment the distinction between ΔH_f° and $\Delta H_{f_{298}}^\circ$). By contrast, Burgers and Holmes²⁶ deduced $\Delta H_f^\circ(\text{CH}_3\text{O}^+) = 247 \pm 5$ kcal/mol from a somewhat complicated argument. First, they showed that the " CH_3O^+ " ions previously believed to be produced by dissociative ionization of CH_3ONO and $(\text{CH}_3)_2\text{O}$ were really CH_2OH^+ , and consequently earlier (lower) heats of formation of CH_3O^+ based on these measurements were invalid. They then prepared CH_3O^+ by charge reversal (starting with CH_3O). Upon measuring the metastable peak from the unimolecular decomposition process



they found that it had the same shape (i.e., the same kinetic energy release) as that from $\text{CD}_3\text{OD}^+ \rightarrow [\text{D}_2\text{COD}^+] \rightarrow \text{DCO} + \text{D}_2$. Consequently, they argued that the transition state for formation of the DCO^+ metastable was the same, whether starting from CD_3O^+ or D_2COD^+ , and that this transition state was "at or close above the enthalpy of formation of CD_3O^+ ." They measured the appearance potential of the metastable DCO^+ peak from CD_3OD (15.1 ± 0.2 eV) which, together with literature values for $\Delta H_f^\circ(\text{CD}_3\text{OD})$ and $\Delta H_f^\circ(\text{H})$, leads to a heat of formation of the transition state of 247 ± 5 kcal/mol. More recently, Ferguson, et al.²⁷ made an estimate of $\Delta H_f^\circ(\text{CH}_3\text{O}^+)$ which provided some support for the value deduced by Burgers and Holmes. The argument is again somewhat involved, but they infer $\Delta H_f^\circ(\text{CH}_3\text{O}^+) = 245 \pm 6$ kcal/mol.

If $\Delta H_f^\circ(\text{CH}_3\text{O})$ is -4 kcal/mol, then these latter inferences regarding $\Delta H_f^\circ(\text{CH}_3\text{O}^+)$ imply I.P. (CH_3O) $\cong 10.5$ eV, very different from Dyke's 7.37 ± 0.03 eV. The major purpose of the current research was to resolve this huge discrepancy.

II. EXPERIMENTAL ARRANGEMENT

The experimental apparatus is a vacuum ultraviolet (VUV) photoionization mass spectrometer. It consists of a VUV light source (in this case, the emission spectrum from an electric discharge in molecular hydrogen), a 3-m VUV monochromator, a chamber where the gas to be studied is crossed by the light exiting from the monochromator, some ion optics and a quadrupole mass spectrometer. The apparatus operates windowless, with differential pumping, and hence can be utilized to much higher photon energies. The VUV light is monitored by a bare photomultiplier, while the ions strike another bare multiplier and are pulse counted. The data consist of ion intensity (normalized to light intensity) as a function of wavelength, which we refer to as the photoion yield.

Experiments of this sort for stable gases can be performed routinely. Transient species present more serious problems, because the number density is much smaller, and the methods of producing these transient species may generate additional noise. We have prepared CH_3O and CH_2OH by the reaction of F atoms with CH_3OH . Several previous studies have shown that H atom abstraction occurs at both the C and O position. McCauley et al.²⁸ have recently studied this reaction, and review earlier results.

A schematic drawing of the apparatus for generating transient species *in situ* near the region of photoionization has been described previously.²⁹ In order to distinguish between CH_2OH and CH_3O , we have used isotopic variants of methanol, particularly CD_3OH and CH_3OD . With CD_3OH , CD_3O^+ occurs at $m/e = 34$, and CD_2OH^+ at $m/e = 33$; with CH_3OD , CH_3O^+ occurs at $m/e = 31$, CH_2OD^+ at $m/e = 32$.

III. EXPERIMENTAL RESULTS

A. The F + CD₃OH reaction

1. CD₂OH⁺, M33

The photoion yield curve of M33, presumed to be CD₂OH⁺ (CD₂OH), displays at least 3 sloping step-like features. They correspond in energy (approximately) to the positions of the peaks in Dyke's²⁵ photoelectron spectrum of CD₂OH. Hence, the dominant ionization process appears to be direct ionization. The half-rise of the first step occurs at $1644.3 \pm 3 \text{ \AA} \equiv 7.540 \pm 0.006 \text{ eV}$, which we take to be the adiabatic I.P. of CD₂OH. Dyke gives $7.55 \pm 0.01 \text{ eV}$ for this quantity. In Dyke's spectrum (and also in ours), there is a weak peak (background in ours) at $\sim 7.4 \text{ eV}$. In order to distinguish between a still lower threshold and a hot band, we performed a simple quasi-diatomic Franck-Condon calculation, assuming harmonic behavior and a frequency (presumed to be C-O⁺) of 1610 cm^{-1} , taken from Dyke. From the relative peak intensities, we calculate a change in bond length of 0.12 \AA . Whangbo, et al.³⁰ have computed a contraction of 0.13 \AA in the C-O bond length between CH₂OH and CH₂OH⁺, in excellent agreement. Alternatively, if we assign the 0→0 peak as 0→1, we can calculate the intensity expected at the 0→0 position. The intensity of the weak peak at $\sim 7.4 \text{ eV}$ is about a factor 5 lower than the predicted intensity and the overall fit for higher peaks becomes much poorer. Hence, this weak feature is attributed to a hot band.

2. CD₃O, M34

The photoion yield curve of M34, presumed to be CD₃O⁺ (CD₃O), displays a broad underlying "background," but an abrupt increase in ion yield occurs at $1155.9 \pm 0.9 \text{ \AA} \equiv 10.726 \pm 0.008 \text{ eV}$. We take this to be the adiabatic I.P. of CD₃O. The underlying background has about the same shape as CD₂OH⁺ from CD₂OH, but is about a factor 20 weaker. A possible source of this background may be the F + CD₃OH reaction itself, where some CD₂OD may be formed. Beyond threshold, one can observe sloping, step-like features with intervals of $\sim 2400 \text{ cm}^{-1}$.

B. The F + CD₃OD, CH₃OD and CH₃OH reactions.

Some of these experiments are still in progress; consequently, these are preliminary results. The F + CD₃OD reaction yields CD₃O, and photoionization produces CD₃O⁺ with essentially the same onset as obtained in the F + CD₃OH experiment. However, in the F + CD₃OD experiment CD₂OD is also formed, and its subsequent ionization yields ion intensity at the same mass, but at lower energy. Hence, CD₃O is identified as an increase in the photoion yield at $m/e = 34$, above that due to CD₂OD⁺.

An adiabatic onset for CH₃O⁺ is not observed at the wavelength expected in the F + CH₃OD and F + CH₃OH experiments. Some ionization at $m/e = 31$ is observed at shorter wavelength (higher photon energy). From zero point energy considerations,²¹ the adiabatic I.P. of CH₃O should be the same as CD₃O, within about 0.001 eV. Hence, the absence of CH₃O⁺ at the expected wavelength implies that it is unstable. In fact, HCO⁺ is observed in this case, in the approximate abundance expected for the decomposition $\text{CH}_3\text{O}^+ \rightarrow \text{HCO}^+ + \text{H}_2$. The adiabatic I.P. of CH₂OH is found to be $1641.5 \pm 1.3 \text{ \AA} \equiv 7.549 \pm 0.006 \text{ eV}$.

IV. DISCUSSION OF RESULTS

A. CH₂OH - CH₂OH⁺

The adiabatic I.P. of CH₂OH obtained in this study ($7.549 \pm 0.006 \text{ eV}$) is very nearly the same as that reported by Dyke^{24,25} ($7.56 \pm 0.01 \text{ eV}$) by photoelectron spectroscopy. Taking $\Delta H^\circ_f(\text{CH}_2\text{OH}^+) \leq 172.0 \pm 0.7 \text{ kcal/mol}$, we deduce $\Delta H^\circ_f(\text{CH}_2\text{OH}) \leq -2.1 \pm 0.7 \text{ kcal/mol}$, or $\Delta H^\circ_{f,298}(\text{CH}_2\text{OH}) \leq -3.7 \pm 0.7 \text{ kcal/mol}$, which is at the upper end of the range given in the Introduction.

B. CD₃O - CD₃O⁺

The I.P. for CD₃O obtained here (10.726 ± 0.008 eV) is obviously very different from Dyke's²⁵ 7.37 ± 0.03 eV. Dyke's experiment consisted of measuring the photoelectron spectrum of the pyrolysis products from dimethyl peroxide. The spectrum is suggestive of a blurred CH₂OH spectrum, but further speculation on our part is unwarranted. If we take $\Delta H_{\text{f}}^{\circ}(\text{CH}_3\text{O}) = 4.0 \pm 1$ kcal/mol, then $\Delta H_{\text{f}}^{\circ}(\text{CH}_3\text{O}) = 5.9 \pm 1$ kcal/mol, and $\Delta H_{\text{f}}^{\circ}(\text{CH}_3\text{O}^+)$ becomes 253.2 ± 1 kcal/mol (251.2 ± 1 at 298 °K). This latter value is within the range deduced by Burgers and Holmes²⁶ (247 ± 5) and estimated by Ferguson, et al.²⁷ (245 ± 6 kcal/mol).

C. CH₃O⁺ - CD₃O⁺

Our failure to observe CH₃O⁺, although CD₃O⁺ was observed, suggests that zero point energy differences or tunneling could account for their relative stabilities. According to *ab initio* calculations,^{21,31} the ground state CH₂OH⁺ potential energy surface is a singlet, whereas that of CH₃O⁺ is a triplet. Ionization of CH₃O will strongly favor formation of CH₃O⁺, over CH₂OH⁺, by Franck-Condon considerations. However, CH₃O⁺ will initially be formed more than 3 eV above the ground state of CH₂OH⁺, and above the thermochemical threshold for formation of HCO⁺ + H₂ (which also represents a singlet surface). One can expect that there will be some crossing between the triplet CH₃O⁺ surface and the singlet surface. Spin-orbit interaction should permit some mixing between the triplet and the singlet surface, and hence the crossing will become an avoided crossing, resulting in a potential barrier. In its lowest vibrational state, CD₃O⁺ appears to be stable to decomposition by barrier penetration (on a time scale of $\sim 10^{-5}$ sec) whereas CH₃O⁺ is not. We look forward to the results of future *ab initio* calculations, which may clarify this point.

REFERENCES

1. "Oxidation of Organic Compounds", Advances in Chemistry Series (American Chemical Society, Washington, D.C., 1968), Vols. I, II, III.
2. K. L. Demerjian, J. A. Kerr, and J. G. Calvert, *Adv. Environ. Sci. Technol.* **4**, 1 (1974).
3. T. Amano and H. E. Warner, *Ap. J. Lett.* **342**, L99 (1989).
4. C. S. Dulcey and J. W. Hudgens, *J. Chem. Phys.* **84**, 5262 (1986).
5. D. S. Bomse, S. Dougal, and R. L. Woodin, *J. Phys. Chem.* **90**, 2640 (1986).
6. P. Pagsberg, J. Munk, A. Sillesen, and C. Anastasi, *Chem. Phys. Lett.* **146**, 375 (1988).
7. G. R. Long, R. D. Johnson, and J. W. Hudgens, *J. Phys. Chem.* **90**, 4901 (1986).
8. S. C. Foster, P. Misra, Y.-T. D. Lin, C. P. Damo, C. C. Carter, and T. A. Miller, *J. Phys. Chem.* **92**, 5914 (1988).
9. X. Liu, C. P. Damo, T.-Y. D. Lin, S. C. Foster, P. Misra, L. Yu, and T. A. Miller, *J. Phys. Chem.* **93**, 2266 (1989).
10. J. Kappert and F. Tany, *Chem. Phys.* **132**, 197 (1989).
11. F. R. Cruickshank and S. W. Benson, *J. Phys. Chem.* **73**, 733 (1969).
12. D. M. Golden and S. W. Benson, *Chem. Rev.* **69**, 125 (1969).
13. E. Buckley and E. Whittle, *Trans. Far. Soc.* **58**, 536 (1962).
14. V. P. Glushko, L. V. Gurvich, G. A. Bergman, I. V. Veitz, V. A. Medredev, G. A. Khachkuruzov, and V. C. Yungman, "Termodinamicheskie Cvoistva Individual'nykh Veshchestv, Vol. 1 and 2, Nauka, Moscow, 1978 and 1979.
15. L. Batt, K. Christie, R. T. Milne and A. J. Summers, *Int. J. Chem. Kin.* **6**, 877 (1974).
16. L. D. Batt and R. T. Milne, *Int. J. Chem. Kin.* **6**, 945 (1974).
17. L. Batt and R. D. McCulloch, *Int. J. Chem. Kin.* **8**, 491 (1976).
18. R. Silverwood and J. H. Thomas, *Trans. Far. Soc.* **63**, 2476 (1967).
19. S. Saebø, L. Radom, and H. F. Schaefer III, *J. Chem. Phys.* **78**, 845 (1983).
20. S. M. Colwell, *Theor. Chim. Acta* **74**, 123 (1988).
21. L. A. Curtiss, D. Kock and J. A. Pople, *J. Chem. Phys.* (to be submitted).
22. L. Batt, J. P. Burrows and G. N. Robinson, *Chem. Phys. Lett.* **78**, 467 (1981).
23. K. M. A. Refaay and W. A. Chupka, *J. Chem. Phys.* **48**, 5205 (1968).

24. J. M. Dyke, A. R. Ellis, N. Jonathan, N. Keddar, and A. Morris, *Chem. Phys. Lett.* **111**, 207 (1984).
25. J. M. Dyke, *J. Chem. Soc. Far. Trans. 2* **83**, 69 (1987).
26. P. C. Burgers and J. L. Homes, *Organic Mass Spectrom.* **19**, 452 (1984).
27. E. E. Ferguson, J. Roncin and L. Bonazzola, *Int. J. Mass Spectrom. Ion Proc.* **79**, 315 (1987).
28. J. A. McCaulley, N. Kelly, M. F. Golde, and F. Kaufman, *J. Phys. Chem.* **93**, 1014 (1989).
29. a) S. T. Gibson, J. P. Greene, and J. Berkowitz, *J. Chem. Phys.* **83**, 4319 (1985); b) J. Berkowitz, J. P. Greene, H. Cho, and B. Ruscic, *J. Chem. Phys.* **86**, 1235 (1987).
30. M.-H. Whangbo, S. Wolfe, and F. Bernardi, *Can. J. Chem.* **53**, 3040 (1975).
31. W. J. Bouma, R. H. Nobes, and L. Radom, *Organic Mass Spectrom.* **17**, 315 (1982).

A TIME-DEPENDENT FLAME MODEL UTILIZING THE METHOD OF LINES

H.D. Ladouceur and J.W. Fleming
Chemistry Division, Code 6110, Naval Research Laboratory
Washington, DC 20375-5000

Keywords: flame modeling, time-dependent model, method of lines

ABSTRACT

We have developed a time-dependent flame model to interpret the temporal evolution of various chemical species generated by laser photolysis of a steady-state low-pressure (10 torr) CH_4/O_2 flame. The model includes the effects of diffusion, convection and elementary chemical kinetics. The diffusion and convection terms are represented by finite difference expressions in the species conservation equations which reduce them to a stiff system of ordinary differential equations. The latter system is solved as an initial value problem by Gear's method. The initial conditions on the model are determined by a photolysis mechanism which perturbs concentrations of the steady-state flame. The computations demonstrate the importance in low-pressure flames of mass transport and chemistry in the relaxation of the perturbed state.

I. INTRODUCTION

This paper describes a time-dependent flame model which utilizes the method of lines (MOL)¹. This model was developed to correlate time-dependent relaxation measurements of steady-state CH_4/O_2 flames perturbed by laser photolysis. The conservation of various chemical species mass fractions (Y_i) within the flame is described by a system of coupled nonlinear partial differential equations² (PDEs) which depend upon the position, x , relative to the burner surface and the time, t . This system of PDEs and the associated boundary conditions are first discretized in the spatial variable by finite-difference formulae. Thus, the system of PDEs is reduced to a system of coupled ordinary differential equations (ODEs) in time. This system of ODEs is readily integrated using Gears method.³

The experiment to be modeled is the 193 nm excimer laser perturbation of a 10 torr CH_4/O_2 flame, $\phi = 0.9$. The OH and CH concentration profiles as well as the temperature profile throughout the flame have been previously reported for the steady-state flame.⁴ In this paper we present the results for OH following perturbation at a position of 3 cm in the post-flame region. As a result of the 193 nm perturbation, the OH concentration increases in the irradiated region. Laser-induced fluorescence is used to monitor OH concentration as it decays back to the steady-state value.

II. MODELING

A. Steady-state flame

We used a one-dimensional flame code⁵, referred to as PREMIX, developed at Sandia for modeling premixed, laminar flames. The code predicts steady-state species spatial profiles from a given set of input variables which include: a chemical mechanism, total pressure, inlet gas composition, mass flux, and a vertical temperature profile. PREMIX uses CHEMKIN-II⁶ and the Sandia thermodynamic data base⁷ to calculate both forward and reverse chemical reaction rates as functions

of pressure, composition and temperature. The mass fluxes due to diffusion are computed from effective binary diffusivities⁸ for the gas mixture utilizing Sandia's Transport Code⁹ and the Lennard-Jones parameters for the various chemical species in the mechanism. Thermal diffusion (Soret effect) is neglected in the present calculations. The boundary conditions are that the mass flux fraction of each specie be specified at the origin and the spatial derivatives of each mass fraction go to zero downstream of the flame region. We chose the chemical mechanism of Miller and Bowman,¹⁰ deleting reactions involving nitrogen. The resulting chemical mechanism consists of 33 chemical species and 150 chemical reactions along with their rate parameters.

The equation governing the spatial distribution of the k^{th} species in a constant pressure, one-dimensional, laminar flame is

$$\rho(\partial Y_k / \partial t) = \dot{\omega}_k W_k - \rho u(\partial Y_k / \partial x) - \partial(\rho Y_k \nabla_k) / \partial x, \quad (1)$$

where Y_k denotes the mass fraction of the k^{th} species ($k=1,33$), x the spatial coordinate, t the time, ρ the mass density, W_k the molecular weight of the k^{th} species, $\dot{\omega}_k$ the molar production rate by chemical reaction of the k^{th} species per unit volume and ∇_k the diffusion velocity of the k^{th} species defined by

$$\nabla_k = v_k - u, \quad (2)$$

where v_k denotes the velocity of the k^{th} species with respect to a stationary coordinate frame and u , the mass-averaged velocity, is given by

$$u(x) = \sum_k Y_k(x) v_k(x). \quad (3)$$

In a burner-stabilized flame, the mass flux (ρu) is a known constant and the molar production rates, $\dot{\omega}_k$, are dependent on the temperature, pressure and composition. These rates are calculated from CHEMKIN-II. The Sandia code solves the steady-state version of Eqn. (1) via a damped Newton method. If convergence difficulties are encountered, a time integration procedure, based upon an Euler algorithm, is implemented to provide a better estimate of the solution. Computations have been carried out on a VAX 6310 computer, where typical computational (CPU) time is less than 30 minutes.

B. TDFLM: Time-dependent flame model

The initial conditions following laser photolysis for the system of ODEs depend upon specific assumptions about the flame and the perturbation laser wavelength. In the post-flame region of our 10 torr CH_4/O_2 flame only H_2O and O_2 have any appreciable absorption at 193 nm. We observe a prompt formation of OH ground-state radicals which relax back to the steady-state with a lifetime of 5 μs . The increased OH, H, and O concentrations and the decreased H_2O and O_2 concentrations from their steady-state values can then be used as the initial conditions for the time-dependent calculation. In the present paper we consider only water photolysis in calculating the initial conditions.

The steady-state flame solutions generated from PREMIX represent the relaxed state of the perturbation experiments. The relaxation after the perturbation is measured in real time and one must have an accurate time-integration scheme to model the experiments. In the MOL algorithm the spatial derivatives on the right-hand side of Eqn. (1) are replaced by finite-difference expressions, reducing the PDEs to a system of ODEs for $Y_k(j,t)$. Each j corresponds to a specified spatial

position above the burner surface. Thus, Eqn. (1) becomes

$$dY_k/dt = \text{Chemistry} - \text{Convection} - \text{Diffusion}, \quad (4)$$

where

$$\text{Chemistry} = \dot{\omega}_k W_k / \rho$$

$$\text{Convection} = u_j [Y_k(j, t) - Y_k(j-1, t)] / [x_j - x_{j-1}]$$

$$\text{Diffusion} = [(\rho Y_k V_k)_{j+1/2} - (\rho Y_k V_k)_{j-1/2}] / [x_{j+1/2} - x_{j-1/2}]$$

Pictorially, this method divides the one-dimensional flame into a number of spatial slices, as represented in Figure 1. The center of each slice corresponds to a particular height above the burner surface. The temporal evolution of the chemical species is computed within each slice along a line parallel to the time axis. This computation is done by Gear's method using DGEAR,³ an IMSL (International Math Science Library) subroutine. The complete solution of these equations requires appropriate boundary conditions and initial conditions. TDFLM computes a starting set of mole fractions at time zero by first reading the steady-state results from the PREMIX calculation for the corresponding position in the flame. The code includes a photolysis mechanism which can alter the concentration of one or more species. The boundary conditions are chosen to correspond to the steady-state PREMIX calculation, i.e., mole fractions are specified upstream (at the burner surface), and spatial derivatives vanish downstream (at the end of the post flame region).

III. DISCUSSION

In the experiment we perturbed a position in the flame 3 cm above the burner surface, which has a measured OH rotational temperature of 1770 ± 60 K, using an ArF excimer laser. The laser beam was masked to produce a measured width of 3 mm and an intensity of 4.0 ± 3.2 J/cm². There is a $117 \pm 15\%$ observed maximum OH concentration increase over the steady-state as a result of the perturbation. This corresponds to photolysis of 7.5% of the water at this height above the burner (based on the PREMIX results). Using temperature dependent absorption coefficients for H₂O and O₂,¹¹ and an observed increase in OH of 117% over the steady-state, the excimer laser intensity is estimated to be 1.2 J/cm². This estimate is consistent with the experimental number. Photolysis of 7.5% of the steady-state water concentration to produce OH and H is utilized as input to the TDFLM code. Concentrations for the perturbed condition are converted to renormalized mass fractions for all chemical species by the TDFLM code. The TDFLM code then calculates the relaxation of the OH concentration back to the steady-state solution. Figure 2 shows the experimental OH decay following the 193 nm laser perturbation (open circles). The experimental steady-state solution is indicated by the filled square, with $\pm 2\sigma$ experimental uncertainty. As can be seen in Figure 2, the OH concentration returns to its steady-state within 15 μ s. The filled circles in Figure 2 are a least-squares fit of the experimental data to a single exponential. Error bars on the least-squares fit are a $\pm 1\sigma$ confidence limit. Figure 3 shows the results of the TDFLM calculation. The axis on the left is the same as Figure 2. The right axis in Figure 3 corresponds to the calculated OH concentration. The filled circles in this figure are taken from Figure 2. The dashed line in Figure 3 results from dropping the diffusion and convection terms in Eqn. (4).

This calculation predicts the OH concentration to decay to a value which is larger than the PREMIX steady-state value. Separate numerical calculations demonstrate that chemistry dominates the short time relaxation. However, in the long time limit the purely kinetic calculation predicts an equilibrium concentration which is slightly greater than the experimentally observed value.

The solid line in Figure 3 is calculated from Eqn. (4) where terms for diffusion, convection and chemistry are included in the calculation. The agreement between the calculated behavior and the experimental observation is good. The binary diffusion coefficient for most gases at 1 atm pressure is on the order of $0.1 \text{ cm}^2/\text{s}$.¹² The diffusion coefficient increases with temperature ($T^{3/2}$ dependence) and is inversely proportional to pressure.¹³ At 1770 K and 10 torr, diffusion coefficients are on the order of $1000 \text{ cm}^2/\text{s}$. Neglecting the diffusion and convection terms in the calculation is equivalent to assuming a homogeneous gas-phase reaction at 1770 K in a closed system. The relative OH concentration decreases more rapidly when mass transport effects are included in Eqn. (4). In the long time limit these terms contribute to a steady-state balance which lies within the error bars of the experiment. At this position in the post-flame, the OH concentration gradient is relatively small, and the net effects of the transport terms is less than 10%.

Future studies will examine the effect of including the photolysis of O_2 in the perturbation mechanism. Also, calculations to model perturbation in the flame zone are planned. In the flame zone, large concentration gradients make the transport terms more important and essential for modeling the observed relaxation.

IV. ACKNOWLEDGEMENTS

We would like to thank Robert Kee and Sandia National Laboratories for providing the Sandia codes.

V. REFERENCES

1. Galant, S., Eighteenth Symposium (International) on Combustion, (The Combustion Institute, 1981) pp 1451-1459.
2. Kuo, K.K., Principles of Combustion, (John Wiley & Sons, New York, 1986) ch. 3.
3. Gear, C.W., "The Automatic Integration of Ordinary Differential Equations", *Comm. A.C.M.*, 14, pp 176-179 (1971). See also IMSL, User's Manual, Vol. 1, Edition 9.2, IMSL Inc., 7500 Bellaire Boulevard, Houston, TX, U.S.A. (1984).
4. Fleming, J.W., Burton, K.A., and Ladouceur, H.D., "OH and CH profiles in a 10 Torr methane/oxygen flame: experiment and flame modeling," *Chem. Phys. Lett.* 175 (4), 395-400 (1990).
5. R.J. Kee, J.F. Grcar, M.D. Smooke, and J.A. Miller, "A Fortran Program for Modeling Steady Laminar One-Dimensional Premixed Flames," Sandia Report SAND85-8240 (1987).
6. R.J. Kee, F.M. Rupley, and J.A. Miller, "Chemkin-II: A Fortran Chemical Kinetics Package for the Analysis of Gas-Phase Chemical Kinetics," Sandia Report SAND 89-8009 (1989).
7. R.J. Kee, F.M. Rupley, and J.A. Miller, "The CHEMKIN Thermodynamic Data Base," Sandia Report SAND87-8215 (1989).
8. Curtis, C.F. and Hirshfelder, J.O., "Transport Properties of Multicomponent Gas Mixtures," *J. Chem. Phys.*, 17, p 550-555 (1949).
9. R.J. Kee, J. Warnatz, and J.A. Miller, "A FORTRAN Computer Code

- Package for the Evaluation of Gas-Phase Viscosities, Conductivities, and Diffusion Coefficients," Sandia Report SAND 83-8209 (1983).
10. Miller, J.A. and Bowman, C.T., "Mechanism and Modeling of Nitrogen Chemistry in Combustion," Prog. Energy Combust. Sci. 15, pp 287-338 (1989).
 11. Davidson, D.F., Chang, A.Y., Kohse-Höinghaus, K., and Hanson, R.K., "High Temperature Absorption Coefficients of O₂, NH₃, and H₂O for Broadband ArF Excimer Laser Radiation," J. Quant. Spectrosc. Radiat. Transfer, 42, No. 4, pp 267-278 (1989).
 12. Bird, R.B., Stewart, W.E., and Lightfoot, E.N., Transport Phenomena, (John Wiley and Sons, New York, 1960) p 503.
 13. *ibid* p 510.

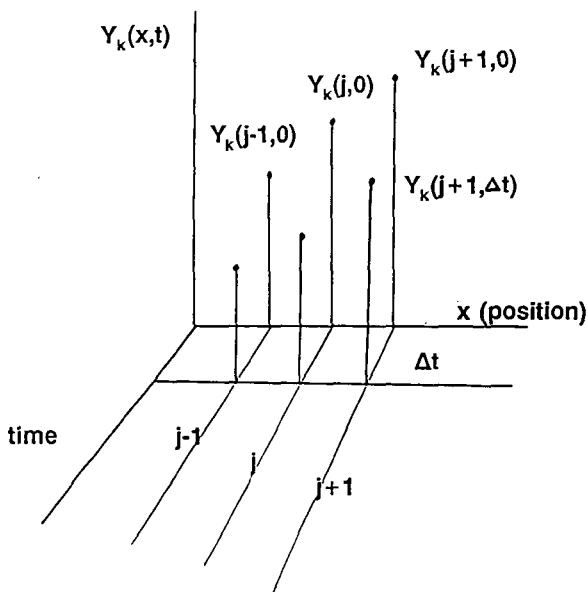


Figure 1. Schematic for the method of lines algorithm. Y_k denotes the k^{th} species mass fraction at position j above the burner at time t .

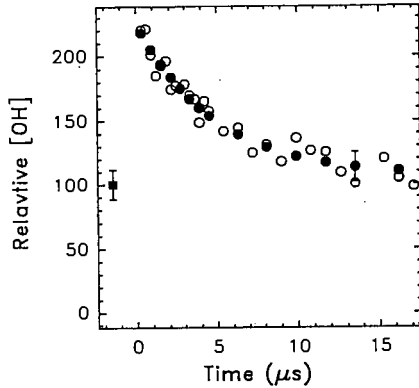


Figure 2. Relative experimental OH concentration at 3 cm above the burner surface in a 10 torr CH_4/O_2 flame as a function of time following 193 nm perturbation (open circles); Least-squares fit of the experimental OH decay to a single exponential (filled circles); relative experimental OH steady-state concentration (filled square). Error bars on the least-squares fit are a $\pm 1\sigma$ confidence limit.

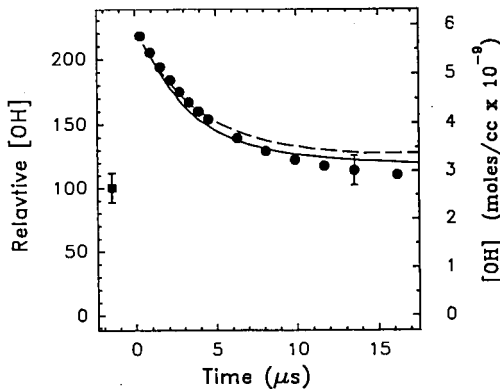


Figure 3. Least-squares fit of the relative experimental OH concentration at 3 cm above the burner surface in a 10 torr CH_4/O_2 flame as a function of time following 193 nm perturbation (filled circles, left axis); relative experimental OH steady-state concentration (filled square, left axis); TDFLM calculation with transport and chemistry (solid line, right axis); TDFLM calculation with no transport terms (dashed line, right axis). Error bars on the experimental steady-state represent $\pm 2\sigma$ experimental uncertainty. Error bars on the least-squares fit are a $\pm 1\sigma$ confidence limit. The left and right vertical axes have been chosen so that the relative experimental steady-state concentration equals the calculated PREMIX value.

CHEMISTRY OF SOLID PROPELLANT COMBUSTION STUDIED BY MASS SPECTROMETRY AND MODELLING.

O.P. Korobeinichev, L.V. Kuibida, A.A. Paletsky, A.A. Chernov, N.E. Ermolin
Laboratory of Kinetics of Combustion Processes
Institute of Chemical Kinetics and Combustion
Novosibirsk 630090, USSR

Keywords: chemistry of combustion, solid propellant, mass spectrometry

ABSTRACT

The flame structure of composite systems containing ammonium perchlorate with particle size $< 50 \mu\text{m}$ and carboxy-terminated polybutadiene binder, component ratio close to stoichiometric (84% AP - 16% CTPB), was studied at a pressure of $8 \cdot 10^3 \text{ Pa}$ using the method of mass-spectrometric probing. The temperature and concentration profiles of 17 stable flame components were determined. Theoretical modelling of this flame structure was carried out by solving the differential equations describing a reacting multicomponent gas flow, involving heat and mass transfer as well as the kinetic mechanism, including 58 elementary steps and 35 components. Satisfactory agreement was achieved between the experimental and calculated data on concentration profiles of most of the 17 stable components and temperature. Rate constants of some little-studied or unstudied steps were estimated. The data obtained may be used to develop a model of the combustion of solid propellants based on ammonium perchlorate.

INTRODUCTION

The study of combustion mechanism at a molecular level is one of the most important problems of the combustion theory of condensed systems (CS). The experimental results on flame structure give the main information about the combustion chemistry, i.e., the kinetics and mechanism of chemical reactions in the combustion wave.

Earlier we have formulated and followed an approach to the study of the combustion chemistry of condensed systems (CS) which combines (a) experimental study of CS flame chemical structure by mass-spectrometric probing with (b) theoretical modelling of this structure by solving equations, describing the reacting multicomponent gas flow, and taking account of the multistep kinetic mechanism.¹⁻⁴ This approach has successfully been used to study the combustion chemistry of AP and RDX,⁴ which made it possible to determine the most significant elementary steps and to estimate the rate constants of some little-studied or unstudied steps. In Reference 5, the above approach was employed to study the combustion chemistry of a homogenized composite solid propellant (CSP), containing ammonium perchlorate (AP) and polybutadiene binder with carboxy-terminated polybutadiene (CTPB) in a 77% AP-23% CTPB ratio of the components (hereafter, this composition will be referred to as composition No. 1) at $6 \cdot 10^4 \text{ Pa}$. The aim of the present paper is to extend these studies. The experimental results are proposed for the flame structure of homogenized composite systems which are close to the stoichiometric ones.

EXPERIMENTAL

Experiments on flame structure were carried out at subatmospheric pressures ($8 \cdot 10^3 \text{ Pa}$) in a helium flow by methods of mass-spectrometric probing of CS flames described in References 1, 2, and 5. The experiments consist of the following: a burning strand of solid fuel is moved toward the probe at a rate exceeding the burning rate, so that the probe is continuously sampling the gaseous species from all the zones including that adjacent to the burning surface. The sample is transported to the ion source of a time-of-flight mass spectrometer. Mass spectra of the sample are recorded with simultaneous filming of the probe and burning surface. The data allow us to identify stable components and to determine their concentrations and spatial distributions, i.e., the flame microstructure.

Apparata of two types have been developed for studying flame structure. In the first type (which was used in this work), a sample is transported to the ion source as a molecular flow. In the second type, the sample is transported to the ion source as a molecular beam.⁴ A quartz cone (exterior and interior angles of 20° and $40\text{-}45^\circ$, respectively) with an orifice diameter of $20 \mu\text{m}$ was used as a

probe; the outer tip diameter was 0.3 mm. The thermal flame structure was studied with the help of microthermocouples (SiO₂-coated platinum and platinum-rhodium wires, 0.02 mm in diameter, and tungsten-rhodium wires, 0.02 mm in diameter) embedded in the propellant samples. A composition of 84% AP (particle size <50 μm) and 16% CTPB (composition No. 2) was used. The sample density was 1.5 g/cm, length - 15 mm, diameter - 8 mm. Cigarette paper served as armoured protection. The burning rate was 0.33 mm/s.

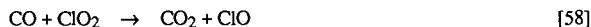
RESULTS AND DISCUSSION

Seventeen stable components (HCl, H₂O, CO, NH₃, CO₂, HClO, NO, O₂, H₂, NO₂, N₂, C₄H₆, C₂H₂, ClO₂, HClO₄, Cl₂, HCN) have been detected using mass-spectrometric probing. Concentration profiles of components in the flame were determined from the experimental data. As a rule, the sensitivity coefficients were estimated from the results of inlet system calibration against individual components. In some cases the mass spectra of combustion product samples and the balance equations for elements were used to determine the HCN and H₂O sensitivity coefficients.

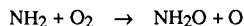
Dots in Fig. 1 (a,b) denote the experimental results from the flame structure, i.e. the dependences of component concentrations and of temperature in the flame under study, plotted as functions of the distance to the burning surface. The data show that the products of CTBP decomposition (C₄H₆, NH₃) are oxidized by those of AP dissociation and decomposition (ClO₂, HClO₄ and HClO) in the 1-mm zone of chemical reactions adjacent to the burning surface. These reactions result in HCl, HCN, C₂H₂, NO, CO, and H₂. The O₂ concentration passes through a maximum; that of Cl₂ decreases monotonically. The ammonia concentration in the combustion products decreases almost to zero, whereas in the combustion products of the fuel-rich composition No. 1, the concentration of ammonia was about 3%.

In Fig. 1(a,b), the solid lines represent the results of flame structure modelling using a stationary solution for the complete set of Navier-Stokes equations for reacting gas.⁴ The experimental values of temperature and component concentrations were used as boundary conditions. In our calculations, we have used an abbreviated kinetic mechanism which involves 58 reversible steps and 35 components (Table 1),⁵ which satisfactorily described the flame structure from composition No. 1. This mechanism has been isolated out of a complete one (258 reversible steps, 49 components).

Analysis of the data obtained shows that in the vicinity of the burning surface, the temperature gradient and the combustion zone width are especially sensitive to variations in the reaction rate constants of the following reactions:



The most important step is the branching reaction 15. This reaction was studied experimentally in a number of papers, and its rate constant is most often taken from the paper by Dean.⁶ However, to reach an agreement between experiment and theory, a rate constant that is 30-times higher must be used. In his recent paper, Dean⁷ proposed another way:



with the rate constant close to our value. There is a satisfactory agreement between experimental and calculated results of the flame structure under investigation. A better agreement with experiment can be achieved by increasing the rate constants for reactions 41 and 58 (see the Table) by 3 and 5 times. Note that the preexponential factors of these reactions are about 10 times as large as those of the same reactions used to calculate the flame structure of the composition No. 1 (with the equal rate constant of the other steps). In order to describe the experimental data on the flame structure of the different composition at various pressures, the mechanism presented in the Table should be improved. Having analyzed the data obtained, we can propose a scheme (Fig. 2) for the transformations of the main initial components (NH₃, C₄H₆, HClO₄, ClO₂) resulting from the reaction of oxidizer and fuel in the condensed phase in the AP-CTPB flame. This simplified scheme allows one to understand the main features of the chemical processes in the flame under consideration.

REFERENCES

1. Korobeinichev, O. P., *Fiz. Goreniya Vzryva* **1987**, *23*, No 5, 64.
2. Ermolin, N. E.; Korobeinichev, O. P.; Tereshchenko, A. G.; et al., *Fiz. Goreniya Vzryva* **1982**, *18*, No. 1, 46.
3. Ermolin, N. E.; Korobeinichev, O. P.; Tereshchenko, A. G.; et al., *Fiz. Goreniya Vzryva* **1982**, *18*, No. 2, 64.
4. Ermolin, N. E.; Korobeinichev, O. P.; Kuibida, L. V.; et al., *Fiz. Goreniya Vzryva* **1986**, *22*, No 5, 54.
5. Korobeinichev, O. P.; Chernov, A. A.; Emel'yanov, I. D.; et al., *Fiz. Goreniya Vzryva* **1990**, *26*, No. 3, 46.
6. Dean, A. M.; et al. *19th Symp. (Intern.) on Comb.*, Pittsburgh: The Combustion Institute, 97 (1982).
7. Dean, A. M.; Bozzelli, J. W. *J. Phys. Chem.* **1982**, *93*, 1058.

Table 1. Rate coefficients in form $k_f = AT^b \exp(-E/RT)$, Ref. 5. Units are mol, cm³, sec, K and cal/mol.

| No. | Reaction | A | b | E |
|-----|--|----------|------|-------|
| 1. | $\text{HClO}_4 \rightarrow \text{ClO}_3 + \text{OH}$ | 1.00E+11 | 0.0 | 39100 |
| 2 | $\text{HClO}_4 + \text{HNO} \rightarrow \text{ClO}_3 + \text{NO} + \text{H}_2\text{O}$ | 3.00E+13 | 0.0 | 6000 |
| 3 | $\text{HClO}_4 + \text{HCO} \rightarrow \text{ClO}_3 + \text{CO} + \text{H}_2\text{O}$ | 5.00E+13 | 0.0 | 0 |
| 4 | $\text{HClO}_4 + \text{HCO} \rightarrow \text{ClO}_2 + \text{CO}_2 + \text{H}_2\text{O}$ | 1.50E+12 | 0.0 | 0 |
| 5. | $\text{ClO}_3 \rightarrow \text{ClO} + \text{O}_2$ | 1.70E+12 | 0.5 | 0 |
| 6. | $\text{Cl} + \text{O}_2 + \text{M} \rightarrow \text{ClO}_2 + \text{M}$ | 6.00E+11 | 0.0 | 11200 |
| 7. | $\text{ClO} + \text{NO} \rightarrow \text{Cl} + \text{NO}_2$ | 6.80E+12 | 0.0 | 311 |
| 8. | $\text{ClOH} + \text{ClO} \rightarrow \text{Cl}_2 + \text{HO}_2$ | 1.00E+14 | 0.0 | 10000 |
| 9. | $\text{ClOH} + \text{OH} \rightarrow \text{ClO} + \text{H}_2\text{O}$ | 1.80E+13 | 0.0 | 0 |
| 10. | $\text{HCl} + \text{OH} \rightarrow \text{Cl} + \text{H}_2\text{O}$ | 5.00E+11 | 0.0 | 750 |
| 11. | $\text{Cl}_2 + \text{H} \rightarrow \text{HCl} + \text{Cl}$ | 8.40E+13 | 0.0 | 1150 |
| 12. | $\text{NH}_3 + \text{ClO} \rightarrow \text{NH}_2 + \text{ClOH}$ | 4.24E+11 | 0.5 | 6400 |
| 13. | $\text{NH}_3 + \text{Cl} \rightarrow \text{NH}_2 + \text{HCl}$ | 4.50E+11 | 0.5 | 100 |
| 14. | $\text{NH}_3 + \text{OH} \rightarrow \text{NH}_2 + \text{H}_2\text{O}$ | 1.00E+11 | 0.68 | 1100 |
| 15. | $\text{NH}_2 + \text{O}_2 \rightarrow \text{HNO} + \text{OH}$ | 6.00E+9 | 0.5 | 0 |
| 16. | $\text{NH}_2 + \text{NO} \rightarrow \text{N}_2 + \text{H}_2\text{O}$ | 2.40E+11 | 0.0 | 0 |
| 17. | $\text{NH}_2 + \text{NO} \rightarrow \text{N}_2\text{H} + \text{OH}$ | 6.00E+11 | 0.0 | 0 |
| 18. | $\text{N}_2\text{H} + \text{NO} \rightarrow \text{HNO} + \text{N}_2$ | 5.00E+13 | 0.0 | 0 |
| 19. | $\text{HNO} + \text{OH} \rightarrow \text{NO} + \text{H}_2\text{O}$ | 3.60E+13 | 0.0 | 0 |
| 20. | $\text{HNO} + \text{O}_2 \rightarrow \text{NO}_2 + \text{OH}$ | 1.00E+13 | 0.0 | 10000 |
| 21. | $\text{HNO} + \text{H} \rightarrow \text{H}_2 + \text{NO}$ | 1.00E+12 | 0.5 | 900 |
| 22. | $\text{NO} + \text{H} + \text{M} \rightarrow \text{HNO} + \text{M}$ | 3.20E+15 | 0.0 | -600 |
| 23. | $\text{N}_2 + \text{HO}_2 \rightarrow \text{HNO} + \text{NO}$ | 8.00E+10 | 0.5 | 41800 |
| 24. | $\text{NO} + \text{HO}_2 \rightarrow \text{NO}_2 + \text{OH}$ | 3.00E+12 | 0.5 | 1800 |

| | | | | |
|-----|--|----------|------|-------|
| 25. | $\text{NO}_2 + \text{H} \rightarrow \text{NO} + \text{OH}$ | 5.00E+14 | 0.0 | 1740 |
| 26. | $\text{H}_2 + \text{OH} \rightarrow \text{H}_2\text{O} + \text{H}$ | 1.00E+8 | 1.6 | 3290 |
| 27. | $\text{C}_4\text{H}_6 + \text{OH} \rightarrow \text{n-C}_4\text{H}_5 + \text{H}_2\text{O}$ | 5.00E+12 | 0.68 | 1100 |
| 28. | $\text{C}_4\text{H}_6 + \text{OH} \rightarrow \text{i-C}_4\text{H}_5 + \text{H}_2\text{O}$ | 5.00E+12 | 0.68 | 1100 |
| 29. | $\text{C}_4\text{H}_6 + \text{ClO} \rightarrow \text{n-C}_4\text{H}_5 + \text{ClOH}$ | 5.00E+12 | 0.5 | 6400 |
| 30. | $\text{C}_4\text{H}_6 + \text{ClO} \rightarrow \text{i-C}_4\text{H}_5 + \text{ClOH}$ | 5.00E+12 | 0.5 | 6400 |
| 31. | $\text{C}_4\text{H}_6 + \text{Cl} \rightarrow \text{n-C}_4\text{H}_5 + \text{HCl}$ | 6.75E+12 | 0.5 | 100 |
| 32. | $\text{C}_4\text{H}_6 + \text{Cl} \rightarrow \text{i-C}_4\text{H}_5 + \text{HCl}$ | 2.25E+11 | 0.5 | 100 |
| 33. | $\text{i-C}_4\text{H}_5 + \text{M} \rightarrow \text{n-C}_4\text{H}_5 + \text{M}$ | 1.00E+14 | 0.0 | 6500 |
| 34. | $\text{n-C}_4\text{H}_5 \rightarrow \text{C}_4\text{H}_4 + \text{H}$ | 5.00E+14 | 0.0 | 45700 |
| 35. | $\text{i-C}_4\text{H}_5 \rightarrow \text{C}_4\text{H}_4 + \text{H}$ | 6.30E+15 | 0.0 | 58700 |
| 36. | $\text{n-C}_4\text{H}_5 \rightarrow \text{C}_2\text{H}_2 + \text{C}_2\text{H}_3$ | 5.00E+13 | 0.0 | 40000 |
| 37. | $\text{i-C}_4\text{H}_5 \rightarrow \text{C}_2\text{H}_3 + \text{C}_2\text{H}_2$ | 6.30E+10 | 0.0 | 32000 |
| 38. | $\text{i-C}_4\text{H}_5 + \text{Cl} \rightarrow \text{C}_4\text{H}_4 + \text{HCl}$ | 1.00E+14 | 0.0 | 1000 |
| 39. | $\text{i-C}_4\text{H}_5 + \text{ClO} \rightarrow \text{C}_4\text{H}_4 + \text{ClOH}$ | 1.00E+14 | 0.0 | 1000 |
| 40. | $\text{C}_4\text{H}_4 + \text{H} \rightarrow \text{C}_2\text{H}_3 + \text{C}_2\text{H}_2$ | 1.30E+14 | 0.0 | 1380 |
| 41. | $\text{C}_4\text{H}_4 + \text{NO}_2 \rightarrow \text{CH}_2 + \text{HCN} + \text{HCO}$ | 5.00E+13 | 0.0 | 0 |
| 42. | $\text{C}_2\text{H}_2 + \text{C}_2\text{H}_2 \rightarrow \text{C}_4\text{H}_4$ | 5.90E+12 | 0.0 | 44600 |
| 43. | $\text{CH}_2\text{CO} + \text{OH} \rightarrow \text{CH}_2\text{O} + \text{HCO}$ | 2.82E+13 | 0.0 | 0 |
| 44. | $\text{CH}_2\text{OO} + \text{NO}_2 \rightarrow \text{CH}_2\text{O} + \text{CO} + \text{NO}$ | 1.00E+13 | 0.0 | 6000 |
| 45. | $\text{C}_2\text{H}_3 + \text{O}_2 \rightarrow \text{CH}_2\text{O} + \text{HCO}$ | 6.00E+13 | 0.0 | 0 |
| 46. | $\text{C}_2\text{H}_2 + \text{H} \rightarrow \text{C}_2\text{H}_3$ | 5.50E+12 | 0.0 | 2330 |
| 47. | $\text{C}_2\text{H}_2 + \text{OH} \rightarrow \text{CH}_3 + \text{CO}$ | 2.00E+12 | 0.0 | 7000 |
| 48. | $\text{CH}_2\text{O} + \text{M} \rightarrow \text{CO} + \text{H}_2 + \text{M}$ | 2.50E+15 | 0.0 | 28600 |
| 49. | $\text{CH}_4 + \text{Cl} \rightarrow \text{CH}_3 + \text{HCl}$ | 2.50E+13 | 0.0 | 3830 |
| 50. | $\text{CH}_4 + \text{ClO} \rightarrow \text{CH}_3 + \text{ClOH}$ | 6.00E+11 | 0.5 | 5700 |
| 51. | $\text{CH}_4 + \text{H} \rightarrow \text{CH}_3 + \text{H}_2$ | 2.20E+4 | 3.0 | 8520 |
| 52. | $\text{CH}_4 + \text{OH} \rightarrow \text{CH}_3 + \text{H}_2\text{O}$ | 1.60E+6 | 2.1 | 2460 |
| 53. | $\text{CH}_3 + \text{H} \rightarrow \text{CH}_4$ | 6.00E+16 | -1.0 | 0 |
| 54. | $\text{HCO} + \text{OH} \rightarrow \text{CO} + \text{H} + \text{M}$ | 2.50E+14 | 0.0 | 16800 |
| 55. | $\text{HCN} + \text{M} \rightarrow \text{NH}_2 + \text{CO}$ | 2.00E+11 | 0.0 | 0 |
| 56. | $\text{CO} + \text{OH} \rightarrow \text{CO}_2 + \text{H}$ | 4.40E+6 | 1.5 | -740 |
| 57. | $\text{CO} + \text{ClO} \rightarrow \text{CO}_2 + \text{Cl}$ | 3.00E+12 | 0.0 | 1000 |
| 58. | $\text{CO} + \text{ClO}_2 \rightarrow \text{CO}_2 + \text{ClO}$ | 5.00E+10 | 0.0 | 0 |

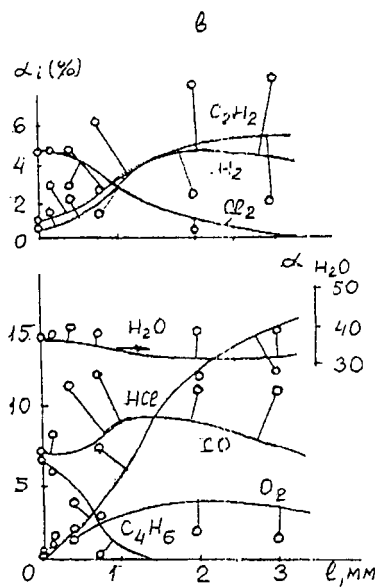
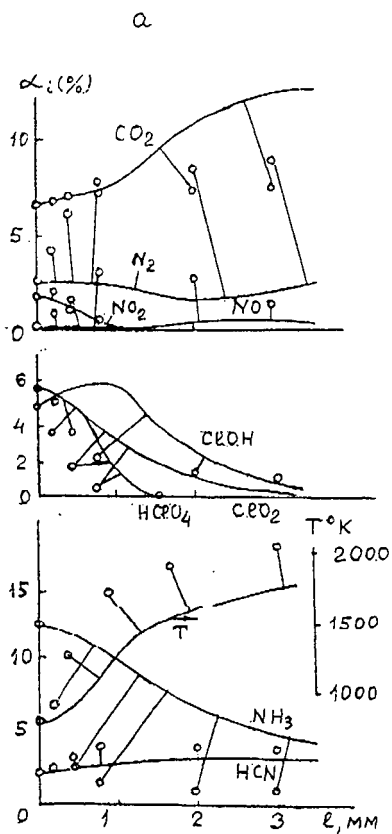


Fig. 1a, b. Temperature and concentrations of stable components in the studied flame vs distance to the burning surface: dots - experiment; solid lines - calculation.

HOMOGENEOUS GAS-PHASE MODELING OF BORON/OXYGEN/HYDROGEN/CARBON COMBUSTION

Louise Pasternack
Chemistry Division, code 6111
Naval Research Laboratory
Washington, D.C. 20375

keywords: boron combustion, combustion model

Introduction

The combustion of boron containing fuels is of importance in propulsion systems because of the potential large release of energy in going from boron to B_2O_3 . The reaction scheme



is exothermic by 467 kcal/mole. The potential energy release from boron containing fuels is considerably greater than from liquid hydrocarbon fuels and from solid fuels containing metallic aluminum. This has resulted in increased attention to fuels composed of liquid hydrocarbons with boron particles suspended in a slurry. Calculations have shown this type of fuel to be an attractive candidate for air breathing propulsion systems which are volume limited.

The calculated advantage of these fuels is based on the assumption of complete combustion to water, carbon dioxide, and liquid B_2O_3 . The combustion of boron containing fuels is a complex process involving both heterogeneous and homogeneous chemistry. First, the boron particles must be volatilized in heterogeneous processes to form gaseous boron containing species. These gas phase species then undergo homogeneous gas phase oxidation to form a mixture of boron oxide and boron oxyhydride species. The final step involves the condensation of the cooling product gases to form liquid B_2O_3 . There are two major limitations to extracting the desired performance of these fuels which have been encountered. One is that boron fuel particles are coated with B_2O_3 . This limits the initial vaporization of boron particles since B_2O_3 is difficult to remove either by vaporization or chemical reaction. The second problem is that the condensation of the final combustion products to liquid B_2O_3 may be slow, especially if boron oxyhydrides are formed as relatively long-lived intermediate species. For maximum efficiency of the combustion of boron containing fuels to be achieved, both the oxidation of the boron particles and the condensation to liquid boria must occur in the short residence time available in the system, typically less than 10^{-4} s.

Much attention has been focussed on these problems over the past several years. In this article, the homogeneous gas phase oxidation of boron, boron oxides, and boron oxyhydrides is discussed. In particular, the role of boron oxyhydrides as metastable species which contribute to the reduction of the overall combustion rate is explored. Efforts to understand this aspect of boron combustion have been hampered by the lack of basic thermodynamic and kinetic data on boron containing species. Modeling studies have been undertaken treating the gas phase oxidation step(1,2). This has helped to define some of the important species and reactions which require further study. Experimental and theoretical studies have focussed on the basic thermodynamics(3-5) and gas phase kinetics(6-10) of some of these systems. Using the results of these studies, the earlier model of homogeneous boron assisted combustion has been modified. The impact on the overall rate of combustion of these recent thermodynamic and kinetic measurements is discussed in this article. Several additional key reactions which may also have a significant impact on the model have been identified.

Model

The model used for this study is based on CHEMKIN gas-phase subroutines(11) and the SENKIN program(12) for predicting gas-phase kinetics with sensitivity analysis developed at Sandia. The modeling calculations predict the time dependence of a homogeneous gas-phase reacting mixture, based on a set of reversible or irreversible chemical reactions. As input, the code requires thermodynamic data in the form of polynomial fits to the heat capacities for all the species included in the mechanism. It also requires a list of all relevant chemical reactions, their rates, and initial species concentrations. The output of the calculation is processed using SENK PLOT graphics developed by D. Burgess of NIST.(13)

Species

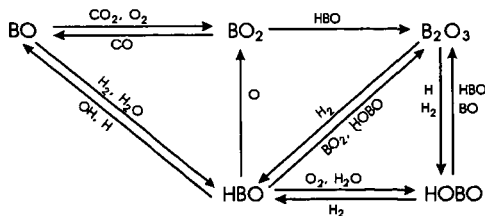
The boron-containing species used in this model include B, BO, BO₂, HBO, B₂O₂(O=B-B=O), B₂O₃(O=B-O-B=O), and HBO₂(H-O-B=O). BH, BH₂, and BOH were also included in some cases. It is assumed that in order to obtain conditions where the B₂O₃ coating on the boron particles is volatilized (T > 1800K), the hydrocarbon fuel is already oxidized. As a result, the H/O/C species used in this model include only H₂, H, O₂, O, OH, H₂O, H₂O₂, HO₂, CO, CO₂, and HCO. N₂ is included as a buffer gas, with total pressure of 1 atm.

Thermodynamics

The thermodynamic data base from Sandia(11) is augmented to include the boron compounds(14). Recently, Page(3) determined the heat of formation of HBO to be -60 kcal/mole using *ab initio* MCSCF with multireference CI techniques. This value of the heat of formation means that HBO is considerably more stable than was previously thought. The most recent JANAF recommended value for the heat of formation was -47.4 ± 3.0 kcal/mole(15). This difference has an impact on the overall boron combustion since HBO becomes a potential metastable species which could act as a bottleneck, preventing rapid combustion to B₂O₃ which is necessary for efficient energy release on the required timescale. The thermodynamic data base has been modified to include the polynomial fit to the thermodynamic properties as determined using statistical mechanics from the geometries, vibrational frequencies and heats of formation calculated by Page for HBO(3). In addition, BOH has been added to the thermodynamic data base, with the values determined in a similar manner.(5)

Kinetic Mechanism

A schematic diagram of the gas phase boron combustion pathways is shown below, which includes only the major species and the pathways which make the largest contributions to their production rates.



For our detailed kinetic mechanism, several modifications to the mechanism of Yetter, et al.(1) have been considered. All the elementary reactions included in the different mechanisms are listed in Table 1. The rates are tabulated in the form $k(\text{cm}^3\text{mol}^{-1}\text{s}^{-1}) = AT^n \exp(-E_a/RT)$. Many of the rate constants for reactions of the boron containing species are taken from reference 1. Most of these values are estimated, since only a few detailed experimental or theoretical values are available. The list of elementary reactions for the hydrogen, oxygen, and carbon species is from Yetter, Dryer, and Rabitz(16) with rates updated to reflect the more recent recommended values of Tsang and Hampson(17).

The change in the heat of formation of HBO results in several exothermic reaction pathways which were previously considered to be endothermic. In particular, the reactions of $\text{BO} + \text{H}_2 \rightarrow \text{HBO} + \text{H}$ and $\text{BO} + \text{OH} \rightarrow \text{HBO} + \text{O}$ are now calculated to be exothermic. The rate of $\text{BO} + \text{H}_2$ reaction has been measured in our laboratory and the rate of $\text{BO} + \text{OH}$ has been calculated from transition state theory. The reaction of $\text{B}_2\text{O}_2 + \text{H} \rightarrow \text{BO} + \text{HBO}$ is also calculated to be exothermic.

Reactions of B with oxidants have been measured at room temperature by DiGiuseppe and Davidovits(18,19). Oldenberg and Baughcum(20) have measured the rate of the $\text{B} + \text{O}_2$ reaction at higher temperatures. Recently, in our laboratory, rates of the reactions of BO with H_2 (6) and O_2 (7) have been measured at temperatures up to 1000K. Transition state theory has also been used to characterize the reactions of $\text{BO} + \text{H}_2$ (3,6) and $\text{BO} + \text{O}_2$ (7). These experimental rates are included in Table 1. We have also used transition state theory to characterize the reaction of $\text{BO} + \text{OH}$.

The remainder of the rate constants are estimated. The rate of reaction of $\text{B}_2\text{O}_2 + \text{H} \rightarrow \text{BO} + \text{HBO}$ is determined by comparison to other B_2O_2 reactions as estimated by Yetter, et al.(1) Several additional B and BO_2 reactions have been added, primarily to include boron hydrides in the kinetics. The rates are determined by analogy to similar reactions listed in reference 1. Reactions of BH have also been included in some of the test mechanisms. The rates of BH with O_2 and H_2O have been measured in our laboratory at temperatures up to 750K.(8) The rate of BH with CO_2 has only been measured at room temperature.(9) We assumed the same activation energy for O_2 and CO_2 reactions. The remainder of the BH reaction rates were estimated. BH_2 is not expected to play a major role in boron combustion; we have included a rate for the hydrogen abstraction from BH_2 by BO in the model which is similar in magnitude to other BO hydrogen abstraction rates.

Reactions have also been added to the mechanism to include the formation and reaction of BOH. Although this radical is not as stable as HBO, it may have a role in the combustion of boron. Rates were determined by comparison to similar reactions involving HBO and BO.

HBO reactions with O_2 and H_2O to form HBO_2 have been added. Several different rates for these reactions have been investigated in alternative mechanisms. The rates of these reactions listed in Table 1 are taken to be the same as Yetter, et al.(1) include for $\text{HBO} + \text{OH} \rightarrow \text{HBO}_2 + \text{H}$. However, the reactions of HBO with O_2 and H_2O involve more rearrangement than the substitution reaction of $\text{HBO} + \text{OH} \rightarrow \text{HBO}_2 + \text{H}$. Consequently, the rates may be slower.

Additional reactions of BO_2 abstracting hydrogen from HBO and HCO have also been included with rates analogous to the $\text{BO}_2 + \text{OH}$ and $\text{BO}_2 + \text{H}_2$ reactions which were included by Yetter, et al.(1) A competing reaction for $\text{BO}_2 + \text{HBO} \rightarrow \text{B}_2\text{O}_3 + \text{H}$ was also included.

Additional HBO_2 removal pathways by reaction with BO and HBO to form B_2O_3 have been added to the mechanism. The reaction with BO can proceed by substitution and its rate is determined by analogy to other similar substitution reactions included in the mechanism. The reaction with HBO is a four center reaction and might be expected to be slower.

Several additional oxidation pathways for $\text{B}_2\text{O}_2 \rightarrow \text{B}_2\text{O}_3$ have been added to the mechanism with rates of $6 \times 10^{11} \text{ cm}^3\text{mol}^{-1}\text{s}^{-1}$. Their actual rates may be slower since these reactions would involve considerable rearrangement of an intermediate.

Results

Several different initial conditions have been considered in order to probe the effects of the different mechanisms and the importance of various reactions on the overall rate of boron combustion. The set of initial conditions listed in reference 2 which were derived from equilibrium calculations on a fuel rich mixture of JP4 and B(s) in air has been used. In addition, initial conditions which test the effects of all the boron being in either the form of HBO or BO have been investigated. The effects of assuming either complete hydrocarbon oxidation with H_2O and CO_2 as the hydrogen and carbon species or incomplete combustion with CO and H_2 as initial species have also been investigated.

In addition to the different initial conditions, several modifications to the mechanism which reflect the additional reactions discussed in the previous section have been studied. The first modification to the model used by Yetter, et al.(1) included the more recent thermodynamic values for HBO and the measured rates of reaction for $BO+H_2$ and $BO+O_2$. The result of these changes is to slow the overall rate of boron combustion, although the final ratio of the concentrations of the boron containing species remains similar. In addition, HBO is shown to be a potential bottleneck in the overall combustion, as can be seen in figure 1a.

This model can be modified by the inclusion of additional HBO removal processes. Adding the reactions of HBO with O_2 and H_2O increases the rate of boron combustion significantly. If the rates are on the order of $10^{12} \text{ cm}^3 \text{ mol}^{-1} \text{ s}^{-1}$, HBO is no longer a metastable species slowing the boron combustion, but instead rapidly converts to HBO_2 , as shown in figure 1b. An analysis of the rate of production of HBO and sensitivity analysis of the combustion process show that these reactions are important and may in fact be controlling, especially $HBO+O_2=HBO_2+O$.

Adding BH reactions has little effect on the overall boron combustion rate since there are few effective pathways to formation of BH under these conditions. Adding reactions involving BOH has no major effect on the overall rate of combustion, although it does play a significant role in the depletion mechanism for BO. BOH is expected to be rapidly oxidized to HBO_2 .

Conclusions

The model for boron combustion has been updated to include recent experimental measurements and theoretical calculations of basic thermodynamic and kinetic data. An examination of the effects of these changes on the overall combustion rate, the production rates of the individual species, and sensitivity analysis has shown that there remain several key reactions which are in need of further study. In particular, reactions of HBO appear to be critical to the overall combustion scheme.

Acknowledgment

The author acknowledges the Office of Naval Research for funding this work through the Naval Research Laboratory.

References

1. Yetter, R. A.; Rabitz, H.; Dryer, F. L.; Brown, R. C.; Kolb, C. E.; Combustion and Flame **1991**, *83*, 43.
2. Brown, R. C.; Kolb, C. E.; Yetter, R. A.; Dryer, F. L.; Rabitz, H. R., "Development of a Boron Assisted Combustion Model with Sensitivity Analysis", Aerodyne Research, Inc., Report No. ARI-RR-580.
3. Page, M., J. Phys. Chem. **1989**, *93*, 3639.
4. Page, M.; Adams, G. F.; Binkley, J. S.; Melius, C. F. J. Phys. Chem. **1987**, *91*, 2676.
5. Page, M., unpublished data.
6. Garland, N. L.; Stanton, C. T.; Nelson, H. H.; Page, M., J. Chem. Phys., submitted.
7. Stanton, C. T.; Garland, N. L.; Nelson, H. H. J. Phys. Chem., submitted.
8. Garland, N. L.; Stanton, C. T.; Fleming, J. W.; Baronavski, A. P.; Nelson, H. H., J. Phys. Chem. **1990**, *94*, 4952.
9. Rice, J. K.; Caldwell, N. J.; Nelson, H. H. J. Phys. Chem. **1989**, *93*, 3600.
10. Pasternack, L.; Balla, R. J.; Nelson, H. H. J. Phys. Chem. **1988**, *92*, 1200.
11. Kee, R. J.; Miller, J. A.; Jefferson, T. H., "CHEMKIN: A General-Purpose, Problem-Independent, Transportable, Fortran Chemical Kinetics Code Package", Sandia, Report No. SAND80-8003.
12. Lutz, A. E.; Kee, R. J.; Miller, J. A. "SENKIN: A Fortran Program for Predicting Homogeneous Gas Phase Chemical Kinetics with Sensitivity Analysis", Sandia, Report No. SAND87-8248.
13. Burgess, D. private communication.
14. Gordon, S.; McBride, B. J., "Computer Program for Calculation of Complex Chemical Equilibrium Compositions, Rocket Performance, Incident and Reflected Shocks, and Chapman-Jouguet Detonations", NASA Report No. NASA SP-273.
15. Chase, M. W. Jr.; Davies, C. A.; Downey, J. R. Jr.; Frurip, D. J.; McDonald, R. A.; Syverud, A. N., J. Phys. Chem. Ref. Data Supp. **1985**, *14*.
16. Yetter, R. A.; Dryer, F. L.; Rabitz, H. "A Comprehensive Reaction Mechanism for the Oxidation of Moist Carbon Monoxide", Fall Western States Section Meeting of the Combustion Institute, WSS Paper 84-96, 1984.
17. Tsang, W.; Hampson, R. F., J. Phys. Chem. Ref. Data **1986**, *15*, 1087.
18. DiGiuseppe, T. G.; Davidovits, P., J. Chem. Phys. **1981**, *74*, 3287.
19. DiGiuseppe, T. G.; Estes, R.; Davidovits, P. J. Phys. Chem. **1982**, *86*, 260.
20. Oldenborg, R. C.; Baughcum, S. L., J. Phys. Chem., submitted.

Table 1. Elementary reactions included in B/O/H/C combustion mechanisms.

| REACTION | A cm ³ /(mol s) | n | Ea cal/mol | REACTION | A | n | Ea |
|----------------|-------------------------------|------|---------------|------------------|---------|-------|---------|
| B+O2=B+O | 7.24E13 | 0.0 | 310. | B0H+OH=B0+H2O | 4.80E13 | 0.0 | 0. |
| B+OH=B+H | 6.05E13 | 0.0 | 0. | B0H+O=BO+OH | 4.80E13 | 0.0 | 0. |
| B+CO2=B+CO | 3.77E10 | 0.0 | 0. | B02+H2=HBO2+H | 1.82E12 | 0.0 | 2980. |
| B+BO2=BBO | 3.43E13 | 0.0 | 0. | B02+OH=HBO2+O | 1.82E12 | 0.0 | 990. |
| B+H2O=BBO+H | 1.00E13 | 0.0 | -1990. | B02+H=HBO2+H | 1.82E12 | 0.0 | 990. |
| B+HCO=BH+CO | 2.40E12 | 0.0 | 2880. | B02+H2=HBO2+H | 1.82E12 | 0.0 | 990. |
| B+H+M=BH+M | 6.03E13 | 0.0 | 0. | B02+HCO=HBO2+CO | 1.82E12 | 0.0 | -1990. |
| B+H2O=BH+H | 1.10E11 | 0.0 | -1990. | B02+HCO2=HBO2+H | 6.03E10 | 0.0 | 9940. |
| B+OH=M+BOH+M | 4.80E12 | 0.0 | 0. | B02+HCO2=HBO2+H | 6.03E10 | 0.0 | 9940. |
| BH+O2=BHO+O | 3.00E13 | 0.0 | -1990. | HBO2+OH=BHO2+H | 4.80E12 | 0.0 | 1990. |
| BH+H2O=BHO+H2 | 3.00E12 | 0.0 | 2400. | HBO2+BO=BHO2+H | 4.80E12 | 0.0 | 0. |
| BH+CO2=BHO+CO | 9.00E11 | 0.0 | 2400. | B2O2+H=BOH+BO | 3.43E13 | 0.0 | 0. |
| BH+O+M=BHO+M | 1.10E15 | 0.0 | -1990. | B2O2+O=BOH+BO2 | 3.43E13 | 0.0 | 0. |
| BH+OH=BHO+H | 3.00E13 | 0.0 | 2400. | B2O2+OH=BOH+HBO2 | 3.43E13 | 0.0 | 0. |
| BH+BO2=BHO+BO | 9.00E11 | 0.0 | 2400. | B2O2+OH=BO2+HBO | 6.03E8 | 0.0 | 69940. |
| BH+HBO2=BHO+H | 3.00E12 | 0.0 | 380. | B2O2+O2=B2O2 | 6.03E8 | 0.0 | 80080. |
| BH2+BO=BHO+BH | 9.00E11 | 0.0 | 2400. | B2O2+OH=B2O3+H | 6.03E11 | 0.0 | 0. |
| HBO+O=BO+H | 4.79E13 | 0.0 | 0. | B2O2+CO2=B2O3+CO | 6.03E11 | 0.0 | 0. |
| HBO+OH=B02+H | 6.03E3 | 0.0 | 70000. | B2O3+OH=HBO2+BO2 | 6.03E11 | 0.0 | 0. |
| HBO+O2=B02+O | 4.79E12 | 0.0 | 70000. | B2O3+H2O=2HBO2 | 6.03E8 | 0.0 | 11920. |
| HBO+H2O=B02+H2 | 4.79E12 | 0.0 | 0. | HCO+H=CO+H2 | 1.21E14 | 0.0 | 0. |
| HBO+OH=B02+H | 4.79E12 | 0.0 | 0. | HCO+O=CO+OH | 3.01E13 | 0.0 | 0. |
| HBO+O+M=B02+M | 4.79E12 | 0.0 | 0. | HCO+O2=HCO2+CO | 5.12E13 | 0.0 | 1690. |
| HBO+H2O=B02+H | 4.79E12 | 0.0 | 0. | HCO2+CO=CO2+OH | 1.51E14 | 0.0 | 23650. |
| HBO+OH=B02+H | 4.79E12 | 0.0 | 0. | CO+OH=CO2+H | 4.39E6 | 1.5 | -740. |
| HBO+O+M=B02+M | 4.79E12 | 0.0 | 0. | CO2+O=CO+O2 | 1.69E13 | 0.0 | 52660. |
| B0+O2=B02+O | 2.42E12 | 0.0 | -507. | H+O2=OH+O | 1.20E17 | -0.91 | 16520. |
| B0+OH=B02+H | 1.10E15 | 0.0 | -1990. | O+H2=OH+H | 5.06E4 | 2.67 | 6290. |
| B0+CO2=B02+CO | 6.03E10 | 0.0 | 9940. | O+H2O=2OH | 4.58E9 | 1.3 | 17100. |
| B0+H2O=B02+H | 4.21E12 | 0.0 | -507. | H+H2O=OH+H2 | 6.19E7 | 1.9 | 18410. |
| B0+OH=B02+H | 3.43E14 | 0.0 | -1990. | O+HCO2=O2+OH | 1.75E12 | 0.0 | 320. |
| B0+H2=BOH+H | 4.32E01 | 3.53 | 3160. | H+HCO2=2OH | 1.69E14 | 0.0 | -400. |
| B0+H+M=BOH+M | 4.32E01 | 3.53 | 3160. | H+HCO2=H2+O2 | 6.62E13 | 0.0 | 2130. |
| B0+H2=BOH+H | 1.64E05 | 2.76 | 5015. | OH+HCO2=H2O+O2 | 5.42E15 | -1.0 | 39740. |
| B0+H2O=BOH+H | 7.92E13 | 0.0 | -1990. | HCO2+O2=HCO2+O | 3.01E13 | 0.0 | 26030. |
| B0+BO2=B02+BO | 4.20E12 | 0.0 | -507. | HCO2+OH=CO+H2O | 1.81E18 | -1.00 | 118100. |
| B0H+CO2=B02+CO | 4.20E12 | 0.0 | -507. | O2+H+O=OH+H | 2.20E14 | 0.0 | 96000. |
| B0H+OH=B02+H | 2.40E15 | 0.0 | -507. | H2O+H=HOH+H | 2.41E15 | 0.0 | 99560. |
| B0H+H2O=B02+H2 | 6.00E10 | 0.0 | 9940. | H2O+H+O=OH+H | 1.29E33 | -4.86 | 53250. |
| B0H+O+M=B02+M | 1.10E15 | 0.0 | -1990. | H2O+H+OH=OH+H | 3.49E15 | 0.0 | 109120. |
| B0H+OH=B02+H | 1.10E15 | 0.0 | -1990. | HCO+H=CO+H | 2.51E13 | -1.18 | 48410. |
| B0H+H2O=B02+H | 4.80E13 | 0.0 | 0. | HCO+OH=CO+H | 5.11E21 | -2.14 | 20420. |
| B0H+O2=B02+O | 4.80E13 | 0.0 | 0. | H+H2O2=H2O+OH | 2.41E13 | 0.0 | 3970. |

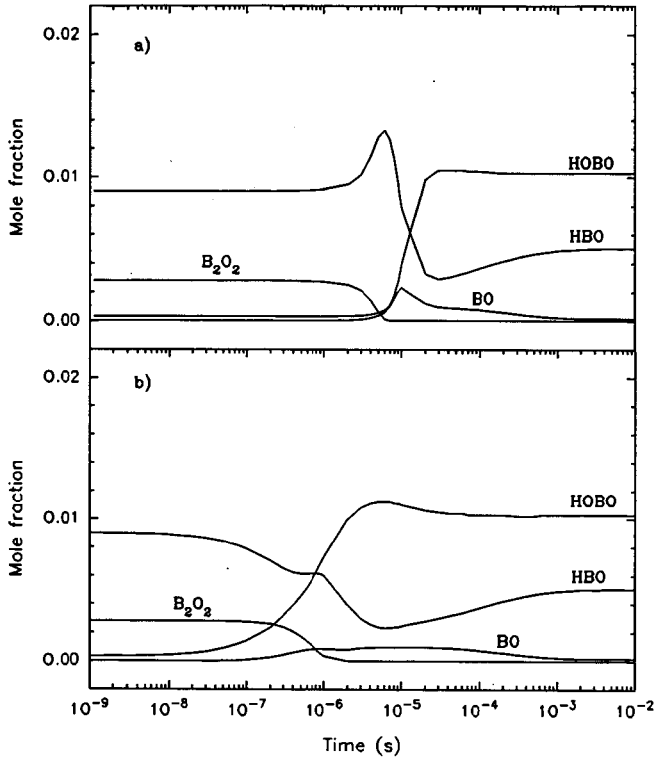


Figure 1. Species profiles as a function of time for an adiabatic, constant pressure (1atm) system. The initial species mole fractions, derived from the equilibrium gas phase calculations of reference 2, are as follows: $X(\text{HBO})=9 \times 10^{-3}$, $X(\text{B}_2\text{O}_2)=2.8 \times 10^{-3}$, $X(\text{B}_2\text{O}_3)=5 \times 10^{-4}$, $X(\text{HBO}_2)=3 \times 10^{-4}$, $X(\text{O}_2)=4.4 \times 10^{-2}$, $X(\text{CO})=0.18$, $X(\text{H}_2)=0.20$, $X(\text{H})=1 \times 10^{-4}$, $X(\text{H}_2\text{O})=1 \times 10^{-5}$, and $X(\text{N}_2)=0.56$, with an initial temperature of 1800K. a) The mechanism includes the more recent thermodynamic value for the heat of formation of HBO and the measured rates of reaction for $\text{BO}+\text{H}_2$ and $\text{BO}+\text{O}_2$, as described in the text. b) Additional HBO removal processes are added to the mechanism.

OXIDATION OF NITROGEN OXIDE IN HOMOGENEOUS GAS PHASE REACTIONS: COMBUSTION EMISSIONS CONTROL MODELING

K. P. Kundu
National Aeronautics and Space Administration
Lewis Research Center
Cleveland, Ohio

J. M. Deur
Sverdrup Technology, Inc.
Lewis Research Center Group
Brook Park, Ohio

Keywords: Nitrogen Oxides, Emissions Control, Modeling

Abstract

An analytical study on the oxidation of NO in homogeneous gas phase reactions is presented. Although NO is readily oxidized to NO₂ at room temperatures, the conversion rate falls with increasing temperature. However, aliphatic alcohols and hydrocarbons generate HO₂ which appears to oxidize NO at higher temperatures. In a medium containing oxygen and aliphatic alcohols or hydrocarbons, NO oxidizes to NO₂ even at 1000 K; but NO₂ returns to NO after these compounds are consumed. Various aliphatic compounds (ethane, butane, methanol, and ethanol) will be considered in this discussion. These chemicals may be useful in the treatment of emissions from stationary combustion systems for removal of NO_x.

Introduction

Nitrogen oxides (NO_x) pose serious environmental concerns due to their role in smog and acid rain formation.(1) These oxides are natural products of combustion, where high temperatures lead to their formation through reactions between dissociated nitrogen and oxygen (thermal NO_x) or through oxidation of nitrogenous compounds created during the combustion process (prompt NO_x). (2,3)

The extent of NO_x formation depends on the initial fuel/air mixture ratio, with greater amounts of NO_x generated with fuel-lean and stoichiometric mixtures. Thus, to control NO_x formation during combustion, one might be tempted to burn a fuel-rich mixture. However, this leads to excessive production of unburned hydrocarbons and carbon monoxide, which also pose severe environmental problems. All of these pollutants can be controlled through careful combustor design (4), but the resultant configuration may have other undesirable characteristics.

Post-combustion treatment of the exhaust to remove NO_x provides an alternative means of reducing the pollution problem. One method introduces various nitrogenous compounds (5-9) into the exhaust stream to react with the NO_x, reducing its concentration. However, this technique is limited to a narrow range of temperatures.(10)

Another post-combustion process removes the NO_x by scrubbing with water. Unfortunately, the poor solubility of most nitrogen oxides precludes direct application of this technique. NO_x is typically comprised of three species: NO, NO₂, and N₂O; and, although nitrogen dioxide (NO₂) is fairly soluble in water, nitrogen oxide (NO) predominates due to the high temperatures associated with combustion. To make the scrubbing technique feasible, the NO needs to be converted to NO₂.(1)

Lyon, et al, improved NO to NO₂ gas phase oxidation through treatment with methanol.(11) The present study expands on this theme by examining NO oxidation in the presence of methanol, ethanol, ethane, and butane.

Physical/Computational Models and Kinetics Mechanisms

Nitrogen oxides are indirect products of combustion, with the extent of formation dependent on temperature and residence time in the combustor. Although combustion is typically complete within a millisecond, NO_x in a fuel-lean mixture grows steadily with time as long as the temperature remains high. However, although equilibrium levels of nitrogen oxides are very high (Fig. 1), NO_x concentrations rarely reach these levels in conventional combustion processes. Thus, while the exhaust stream composition may approach equilibrium in general, the NO_x concentration will not.

The ability of hydrocarbons and alcohols to oxidize NO_x in an exhaust stream that, apart from the NO_x , is at equilibrium will be examined using the LSENS program of Bittker and Radhakrishnan.(12) In particular, the code's plug flow reaction model is used to compute concentrations at various times during the combustion process.

The starting point for these calculations will be the fuel-lean mixture described in Table I. As shown in the table, all of the NO_x is in the form of NO. This follows from the argument that, in the absence of hydrocarbon fragments, any NO_x present would be converted to NO at the high temperatures being considered.

The kinetics mechanism for the calculations (shown in Appendix A) is essentially identical to that of Miller and Bowman (13), with a few species deleted to fit the constraints of the LSENS program. Additional reactions involving methanol, ethanol, and butane are taken from Westbrook and Dryer.(14) Finally, thermodynamic data has been obtained from B. J. McBride (Lewis Research Center) and the Sandia National Laboratory.(15)

Oxidation of NO in the Presence of Methanol

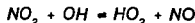
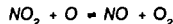
The fractional conversion of NO to NO_2 at various temperatures is shown in Fig. 2. As seen in the observations of Lyon, et al, the oxidation of NO occurs more quickly at higher temperatures.(11)

Hori (16) observed the formation of NO_2 in fuel-rich combustion and suggested that NO was oxidized by HO_2 , while a similar result was reported by Sano (17) in a calculation of a hot gas mixing with cold air. The HO_2 is predominately formed from methyl alcohol and the CH_2OH radical, both products of methanol decomposition.(11) To test these findings, the reaction:



was deleted from the model, and the NO_2 concentration was recalculated. The initial mixture composition was retained, and the initial temperature was set at 1100 K. This temperature was chosen because it had been found previously to result in the rapid formation of NO_2 . With the above reaction removed, however, the formation of NO_2 was now negligible; but, when the forward reaction was restored but not the reverse reaction, significant NO_2 formation again took place. Hence, NO oxidation is dependent on: 1) the formation of HO_2 , and 2) the reaction between HO_2 and NO.

Once all of the alcohol is consumed, NO_2 reverts to NO. This follows from the reactions involved in the chemical reduction of NO_2 :



By varying the rates for the above reactions, it was found that all but the first reaction can reduce the NO_2 concentration. When methanol is consumed, these reactions act to lower the NO_2 concentration. The activity of the reactions also explains why NO_2 concentration is lower at higher temperatures.

To determine if the concentration of methanol has any effect on NO oxidation, the oxidation process was examined at different concentrations of CH_2OH using 1100 K as the reaction temperature. It appears that, in the presence of large amounts of methanol, the speed of the oxidation process increases. Heat is released in such cases, and it has already been noted that NO oxidation occurs more quickly at higher temperatures. However, if the amount of excess methanol is small, the rate of oxidation is not affected. Understandably, since their work did not consider mixtures with large amounts of methanol, Lyon, et al, reported only this latter finding.(11)

The effect of oxygen on NO oxidation in the presence of methanol was also studied. It was determined that increases in O_2 concentration do not affect the rate.

Oxidation of NO in the Presence of Ethanol

Since ethanol and methanol are very similar chemically, it can be expected that ethanol will behave similarly in

the oxidation of NO. Unfortunately, there is no experimental data available; therefore, the choice of the kinetic model is very important to insure the accuracy of the analysis. The mechanism of Westbrook and Dryer was chosen, as it was found to have rate parameters that were very similar to those of the methanol mechanism.

The calculations made with this mechanism showed that ethanol oxidizes NO to NO₂ in a manner identical to methanol. The variations in NO₂ concentration with time and temperature are shown in Fig. 3. As expected, NO₂ formation initially rises with increasing temperature and then falls as the ethanol is consumed.

Oxidation of NO in the Presence of Ethane and Butane

Little experimental data is available on the oxidation of NO in the presence of hydrocarbons. Hori (16) found that, as with methanol and ethanol, hydrocarbon reactions also generate HO₂, while Malte and Kramlich (18) also saw evidence of NO₂ formation. In a similar situation, Jasma and Boreman (19) showed that small amounts of H₂ and CO led to NO to NO₂ conversion, while the first author (20) has demonstrated the use of methane and hydrogen to also promote NO oxidation. Thus, the presence of ethane and butane might boost NO oxidation.

Figs. 4 and 5 show the calculated NO₂ concentration at varying temperatures in the presence of ethane and butane, respectively. As with methanol, the major species involved in the oxidation of NO is HO₂. This was proved using a method similar to that followed in the case of methanol. In fact, it was found that ethane and methanol behave almost identically in the oxidation of NO. When a large amount of ethane is present, there is some reduction of the total NO₂, and the reduction increases at higher temperatures. This reduction is due to reactions involving hydrocarbon fragments.

The effect of adding large amounts of oxygen was also studied. As the oxygen concentration varied from 4% to 12%, NO₂ formation changed by only 10%.

Conclusions

Computer modeling has been used to study the formation of NO in the presence of methanol, ethanol, butane, and ethane. It appears that NO₂ is formed through oxidation of NO by HO₂ which is generated by these additives. The oxidation process is temperature dependent, with higher conversion rates at higher temperatures. However, at all temperatures, the NO₂ begins to revert to NO, once the additives are consumed; but, as long as the additives are present, the oxidation rate is only slightly dependent on the actual additive concentration. Although the presence of oxygen is necessary for the formation of NO₂, excess oxygen does not affect the NO₂ conversion.

References

1. Rosenberg, H. S., Curan, L. M., Slack, A. V., and Oxley, J. H., *Prog. in Energ. and Comb. Sci.*, vol. 6, 1988, p. 287.
2. Zeldovich, Y. B., *Acta Physiochim*, vol. 21, 1946, p. 577.
3. Fennimore, C. P., *Comb. and Flame*, vol. 2, 1976, p. 1.
4. Sarofin, A. F., and Flagan, R. C., *Prog. in Energ. and Comb. Sci.*, vol. 2, 1976, p. 1.
5. Lyon, R. K., *U.S. Patent No. 3900554*, 1975.
6. Turchan, O. C., *U.S. Patent No. 4208386*, 1980.
7. Perry, R. A., *U.S. Patent No. 4731231*, 1988.
8. Arand, J. K., Muzio, L. J., and Scotter, J. G., *U.S. Patent No. 4208386*, 1980.
9. Wada, Y., and Yamatsuta, K., *Japanese Early Disclosure Patent No. 54028771*, 1980.
10. Lyon, R. K., and Benn, D., *17th Sym. (Intl.) on Comb.*, The Combustion Institute, Pittsburgh, 1979, p.601.
11. Lyon, R. K., Cole, J. A., Kramlich, J. C., and Chen, S. L., *Comb. and Flame*, Vol. 81, 1990, p. 30.

12. Radhakrishnan, K., and Bittker, D. A., *Eastern Section, Comb. Inst. Fall Meetings*, December 15-17, 1986.
13. Miller, J. A., and Bowman, C. T., *Prog. in Energy and Comb. Sci.*, Vol. 15, 1989, p. 287.
14. Westbrook, C. K., and Dryer, F. L., *Prog. in Energy and Comb. Sci.*, Vol. 10, 1984, p. 1.
15. Kee, R. J., Rupley, F. M., and Miller, J. A., *SAND87-8215*, 1987.
16. Hori, M., *22nd Sym. (Intl.) on Comb.*, The Combustion Institute, Pittsburgh, 1988, p. 1175.
17. Sano, T., *Comb. Sci. and Tech.*, Vol. 38, 1984, p. 129.
18. Kramlich, J. C., Malte, P. C., *Comb. Sci. and Tech.*, Vol. 18, 1978, p. 91.
19. Jasma, D., and Borman, G., *Comb. Sci. and Tech.*, Vol. 23, 1980, p. 83.
20. Kundu, K. P., Nguyen, H. L., and Kang, M. P., *AIAA 29th Aerospace Sciences Meeting*, Reno, Nevada, 1991.

Table I. Initial Mixture Composition.

| Species | Mole Fraction | Species | Mole Fraction |
|--------------------|---------------|-----------------|---------------|
| O ₂ | 0.0400 | NO | 0.0002 |
| CH ₃ OH | 0.0004 | CO ₂ | 0.0100 |
| H ₂ O | 0.1000 | Ar | 0.0080 |
| N ₂ | 0.8414 | | |

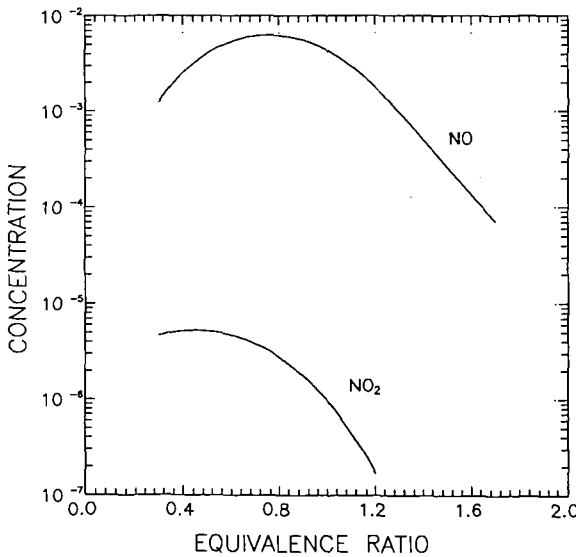


Figure 1. Equilibrium NO and NO₂ Concentrations (T = 800 K, p = 1 atm).

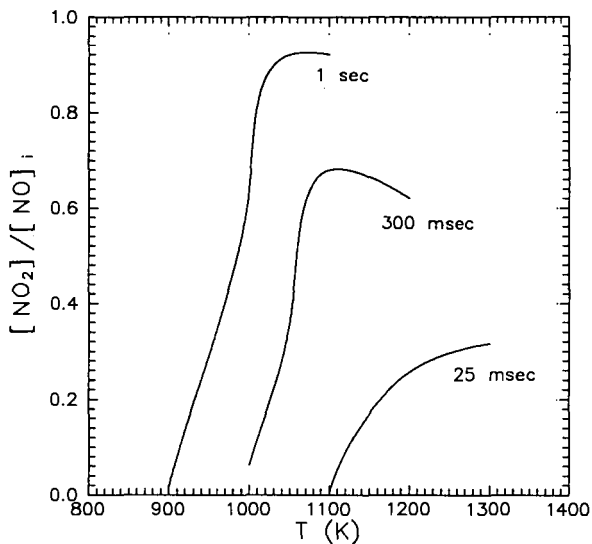


Figure 2. NO Conversion in the Presence of Methanol.

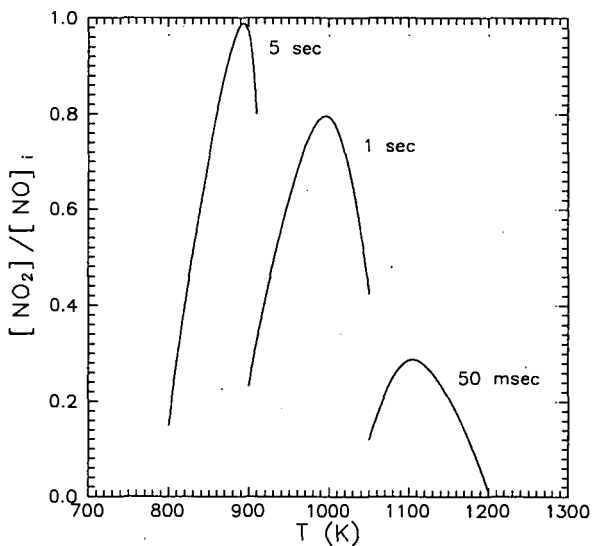


Figure 3. NO Conversion in the Presence of Ethanol.

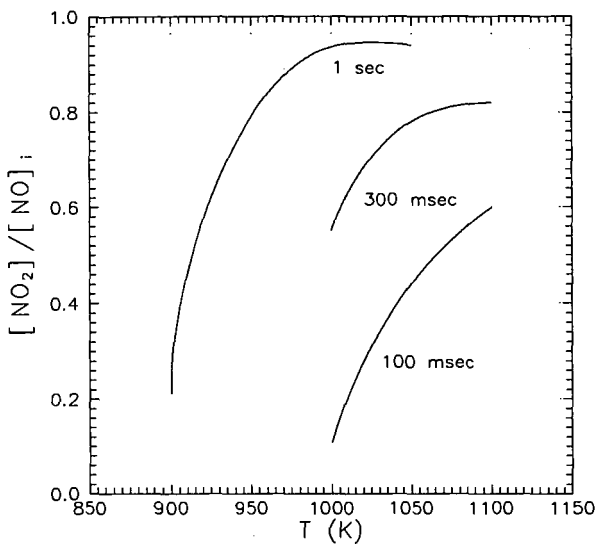


Figure 4. NO Conversion In the Presence of Ethane.

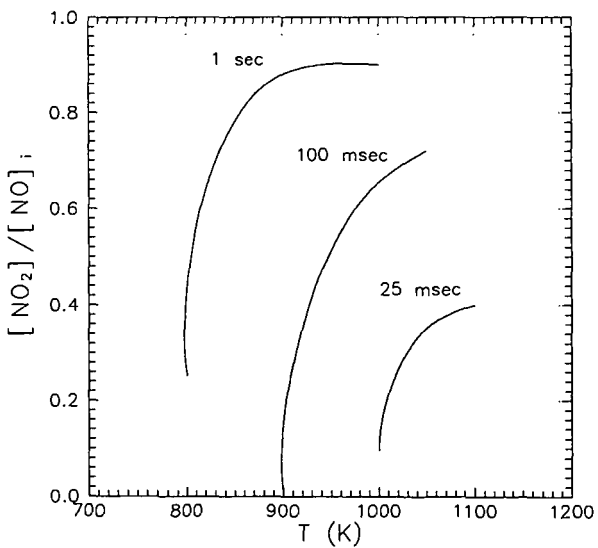


Figure 5. NO Conversion In the Presence of Butane.

Appendix A. Kinetics Mechanism.(13)

$$k = A T^B e^{-C/RT}$$

| REACTION | A | B | C | REACTION | A | B | C |
|---|-----------------------|-------|---------|---|------------------------|------|---------|
| M + 2CH ₃ → C ₂ H ₆ + M | 9.03x10 ¹⁶ | -1.2 | 654.0 | CH + CH ₂ → C ₂ H ₂ + H | 4.00x10 ¹³ | 0.0 | 0.0 |
| CO 2.0, H ₂ 2.0, CO ₂ 3.0, H ₂ O 5.0 | | | | CH + CH ₃ → C ₂ H ₃ + H | 3.00x10 ¹³ | 0.0 | 0.0 |
| CH ₃ + H → CH ₄ + M | 6.00x10 ¹⁶ | -1.0 | 0.0 | CH + CH ₄ → C ₂ H ₄ + H | 6.00x10 ¹³ | 0.0 | 0.0 |
| CO 2.0, H ₂ 2.0, CO ₂ 3.0, H ₂ O 5.0 | | | | C + O ₂ → CO + O | 2.00x10 ¹³ | 0.0 | 0.0 |
| CH ₄ + O ₂ → CH ₃ + HO ₂ | 7.90x10 ¹³ | 0.0 | 56000.0 | C + OH → CO + H | 5.00x10 ¹³ | 0.0 | 0.0 |
| CH ₄ + H → CH ₃ + H ₂ | 2.20x10 ⁰⁴ | 3.0 | 8750.0 | C + CH ₃ → C ₂ H ₂ + H | 5.00x10 ¹³ | 0.0 | 0.0 |
| CH ₄ + OH → CH ₃ + H ₂ O | 1.60x10 ⁰⁶ | 2.1 | 2460.0 | C + CH ₂ → C ₂ H + H | 5.00x10 ¹³ | 0.0 | 0.0 |
| CH ₄ + O → CH ₃ + OH | 1.02x10 ⁰⁹ | 1.5 | 8604.0 | CH ₂ + CO ₂ → CH ₂ O + CO | 1.10x10 ¹¹ | 0.0 | 1000.0 |
| CH ₄ + HO ₂ → CH ₃ + H ₂ O ₂ | 1.80x10 ¹¹ | 0.0 | 18700.0 | CH ₂ + O → 2H + CO | 5.00x10 ¹³ | 0.0 | 0.0 |
| CH ₃ + HO ₂ → CH ₃ O + OH | 2.00x10 ¹³ | 0.0 | 0.0 | CH ₂ + O → CO + H ₂ | 3.00x10 ¹³ | 0.0 | 0.0 |
| CH ₃ + O ₂ → CH ₃ O + O | 2.05x10 ¹⁹ | -1.6 | 29229.0 | CH ₂ + O ₂ → 2H + CO ₂ | 1.60x10 ¹² | 0.0 | 1000.0 |
| CH ₃ + O → CH ₂ O + H | 8.00x10 ¹³ | 0.0 | 0.0 | CH ₂ + O ₂ → CH ₂ O + O | 5.00x10 ¹³ | 0.0 | 9000.0 |
| CH ₂ OH + H → CH ₃ + OH | 1.48x10 ¹⁴ | 0.0 | 0.0 | CH ₂ + O → CO + H ₂ O | 1.90x10 ¹⁰ | 0.0 | -1000.0 |
| M + CH ₂ OH → CH ₂ O + H | 1.00x10 ¹⁴ | 0.0 | 25000.0 | CH ₂ + O ₂ → CO ₂ + H ₂ | 6.90x10 ¹¹ | 0.0 | 500.0 |
| CH ₂ OH + H → CH ₂ O + H ₂ | 2.00x10 ¹³ | 0.0 | 0.0 | CH ₂ + O ₂ → HCO + OH | 4.30x10 ¹⁰ | 0.0 | -500.0 |
| CH ₂ OH + OH → CH ₂ O + H ₂ O | 1.00x10 ¹³ | 0.0 | 0.0 | CH ₂ O + OH → HCO + H ₂ O | 3.43x10 ⁰⁹ | 1.18 | -447.0 |
| CH ₂ OH + O → CH ₂ O + OH | 1.00x10 ¹³ | 0.0 | 0.0 | CH ₂ O + H → HCO + H ₂ | 2.19x10 ⁰⁸ | 1.77 | 3000.0 |
| CH ₂ OH + O ₂ → CH ₂ O + HO ₂ | 1.48x10 ¹³ | 0.0 | 1500.0 | M + CH ₂ O → HCO + H | 3.31x10 ¹⁶ | 0.0 | 81000.0 |
| M + CH ₃ OH → CH ₃ + OH | 3.02x10 ¹⁸ | 0.0 | 80000.0 | CH ₂ O + O → HCO + OH | 1.80x10 ¹³ | 0.0 | 3080.0 |
| H + CH ₃ OH → CH ₃ + H ₂ O | 2.00x10 ¹² | 0.0 | 5300.0 | HCO + OH → H ₂ O + CO | 1.00x10 ¹⁴ | 0.0 | 0.0 |
| H + CH ₃ OH → CH ₂ OH + H ₂ | 3.02x10 ¹³ | 0.0 | 7000.0 | M + HCO → H + CO | 2.50x10 ¹⁴ | 0.0 | 16802.0 |
| OH + CH ₃ OH → CH ₂ OH + H ₂ O | 3.98x10 ¹² | 0.0 | 2000.0 | CO 1.9, H ₂ 1.9, CH ₄ 2.8, CO ₂ 3.0, H ₂ O 5.0 | | | |
| CH ₃ O + H → CH ₃ + OH | 1.00x10 ¹⁴ | 0.0 | 0.0 | HCO + H → CO + H ₂ | 1.19x10 ¹³ | 0.25 | 0.0 |
| CH ₃ OH + O ₂ → CH ₂ OH + HO ₂ | 3.98x10 ¹⁰ | 0.0 | 50910.0 | HCO + O → CO + OH | 3.00x10 ¹³ | 0.0 | 0.0 |
| CH ₃ OH + O → CH ₂ OH + OH | 1.70x10 ¹² | 0.0 | 2290.0 | HCO + O → CO ₂ + H | 3.00x10 ¹³ | 0.0 | 0.0 |
| CH ₃ OH + CH ₃ → CH ₂ OH + CH ₄ | 1.82x10 ¹¹ | 0.0 | 9800.0 | HCO + O ₂ → HO ₂ + CO | 3.00x10 ¹³ | 0.0 | 0.0 |
| CH ₃ OH + HO ₂ → CH ₂ OH + H ₂ O ₂ | 6.31x10 ¹² | 0.0 | 19360.0 | CO + O → CO ₂ + M | 6.17x10 ¹⁴ | 0.0 | 3000.0 |
| CH ₃ + OH → CH ₂ + H ₂ O | 7.50x10 ⁰⁶ | 2.0 | 5000.0 | CO + OH → CO ₂ + H | 1.51x10 ⁰⁷ | 1.3 | -758.0 |
| CH ₃ + H → CH ₂ + H ₂ | 9.00x10 ¹³ | 0.0 | 15100.0 | CO + O ₂ → CO ₂ + O | 1.60x10 ¹³ | 0.0 | 41000.0 |
| M + CH ₃ O → CH ₂ O + H | 1.00x10 ¹⁴ | 0.0 | 25000.0 | HO ₂ + CO → CO ₂ + OH | 5.80x10 ¹³ | 0.0 | 22934.0 |
| CH ₃ O + H → CH ₂ O + H ₂ | 2.00x10 ¹³ | 0.0 | 0.0 | C ₂ H ₆ + CH ₃ → C ₂ H ₅ + CH ₄ | 5.50x10 ⁻⁰¹ | 4.0 | 8300.0 |
| CH ₃ O + OH → CH ₂ O + H ₂ O | 1.00x10 ¹³ | 0.0 | 0.0 | C ₂ H ₆ + O ₂ → C ₂ H ₅ + HO ₂ | 1.00x10 ¹³ | 0.0 | 51000.0 |
| CH ₃ O + O → CH ₂ O + OH | 1.00x10 ¹³ | 0.0 | 0.0 | C ₂ H ₆ + H → C ₂ H ₅ + H ₂ | 5.40x10 ⁰² | 3.5 | 5210.0 |
| CH ₃ O + O ₂ → CH ₂ O + HO ₂ | 6.30x10 ¹⁰ | 0.0 | 2600.0 | C ₂ H ₆ + O → C ₂ H ₅ + OH | 2.51x10 ¹³ | 0.0 | 6360.0 |
| CH ₂ + H → CH + H ₂ | 1.00x10 ¹⁸ | -1.56 | 0.0 | C ₂ H ₆ + OH → C ₂ H ₅ + H ₂ O | 8.70x10 ⁰⁹ | 1.05 | 1810.0 |
| CH ₂ + OH → CH + H ₂ O | 1.13x10 ⁰⁷ | 2.0 | 3000.0 | C ₂ H ₄ + H → C ₂ H ₃ + H ₂ | 1.10x10 ¹⁴ | 0.0 | 8500.0 |
| CH ₂ + OH → CH ₂ O + H | 2.50x10 ¹³ | 0.0 | 0.0 | C ₂ H ₄ + O → CH ₃ + HCO | 3.32x10 ¹² | 0.0 | 1130.0 |
| CH + O ₂ → HCO + O | 3.30x10 ¹³ | 0.0 | 0.0 | C ₂ H ₄ + OH → C ₂ H ₃ + H ₂ O | 2.02x10 ¹³ | 0.0 | 5955.0 |
| CH + O → CO + H | 5.70x10 ¹³ | 0.0 | 0.0 | CH ₂ + CH ₃ → C ₂ H ₄ + H | 3.00x10 ¹³ | 0.0 | 0.0 |
| CH + OH → HCO + H | 3.00x10 ¹³ | 0.0 | 0.0 | M + C ₂ H ₅ → C ₂ H ₄ + H | 2.00x10 ¹⁵ | 0.0 | 30000.0 |
| CH + CO ₂ → HCO + CO | 3.40x10 ¹² | 0.0 | 690.0 | C ₂ H ₅ + H → 2CH ₃ | 1.00x10 ¹⁴ | 0.0 | 0.0 |
| CH + H → C + H ₂ | 1.50x10 ¹⁴ | 0.0 | 0.0 | C ₂ H ₅ + O ₂ → C ₂ H ₄ + HO ₂ | 8.43x10 ¹¹ | 0.0 | 3875.0 |
| CH + H ₂ O → CH ₂ O + H | 1.17x10 ¹⁵ | -0.75 | 0.0 | C ₂ H ₂ + O → CH ₂ + CO | 1.02x10 ⁰⁷ | 2.0 | 1900.0 |
| CH + CH ₂ O → CH ₂ CO + H | 9.46x10 ¹³ | 0.0 | -515.0 | C ₂ H ₂ + O → HCCO + H | 1.02x10 ⁰⁷ | 2.0 | 1900.0 |

| REACTION | A | B | C | REACTION | A | B | C |
|---|------------------------|------|----------|--|-----------------------|------|---------|
| $C_2H_2 + O_2 \rightarrow 2HCO$ | 3.98×10^{12} | 0.0 | 28000.0 | $OH + HO_2 \rightarrow H_2O + O_2$ | 7.50×10^{12} | 0.0 | 0.0 |
| $H_2 + C_2H \rightarrow C_2H_2 + H$ | 1.02×10^{07} | 2.0 | 1900.0 | $H + HO_2 \rightarrow 2OH$ | 1.40×10^{14} | 0.0 | 1073.0 |
| $H + C_2H_2 \rightarrow C_2H_3 + M$ | 5.54×10^{12} | 0.0 | 2410.0 | $O + HO_2 \rightarrow O_2 + OH$ | 1.40×10^{13} | 0.0 | 1073.0 |
| H_2 2.0, CO 2.0, CO_2 3.0, H_2O 5.0 | | | | $2OH \rightarrow O + H_2O$ | 6.00×10^{08} | 1.3 | 0.0 |
| $C_2H_3 + H \rightarrow C_2H_2 + H_2$ | 4.00×10^{13} | 0.0 | 0.0 | $M + 2H \rightarrow H_2 + M$ | 1.00×10^{18} | -1.0 | 0.0 |
| $C_2H_3 + O \rightarrow CH_2CO + H$ | 3.00×10^{13} | 0.0 | 0.0 | $H_2 + 2H \rightarrow 2H_2$ | 9.20×10^{16} | -0.6 | 0.0 |
| $C_2H_3 + O_2 \rightarrow C_2H_2 + HO_2$ | 1.00×10^{12} | 0.0 | 10000.0 | $H_2O + 2H \rightarrow H_2 + H_2O$ | 6.00×10^{19} | -1.2 | 0.0 |
| $C_2H_3 + O_2 \rightarrow CH_2O + HCO$ | 4.00×10^{12} | 0.0 | -250.0 | $H + OH \rightarrow H_2O + M$ | 1.60×10^{22} | -2.0 | 0.0 |
| $C_2H_3 + OH \rightarrow C_2H_2 + H_2O$ | 5.00×10^{12} | 0.0 | 0.0 | H_2O 5.0 | | | |
| $C_2H_3 + CH_2 \rightarrow C_2H_2 + CH_3$ | 3.00×10^{13} | 0.0 | 0.0 | $H + O \rightarrow OH + M$ | 6.20×10^{16} | -0.6 | 0.0 |
| $C_2H_3 + C_2H \rightarrow 2C_2H_2$ | 3.00×10^{13} | 0.0 | 0.0 | H_2O 5.0 | | | |
| $C_2H_3 + CH \rightarrow CH_2 + C_2H_2$ | 5.00×10^{13} | 0.0 | 0.0 | $M + 2O \rightarrow O_2 + M$ | 1.89×10^{13} | 0.0 | -1788.0 |
| $OH + C_2H_2 \rightarrow C_2H + H_2O$ | 3.37×10^{07} | 2.0 | 14000.0 | $H + HO_2 \rightarrow H_2 + O_2$ | 1.25×10^{13} | 0.0 | 0.0 |
| $OH + C_2H_2 \rightarrow CH_2CO + H$ | 2.18×10^{-04} | 4.5 | -1000.0 | $2HO_2 \rightarrow H_2O_2 + O_2$ | 2.00×10^{12} | 0.0 | 0.0 |
| $OH + C_2H_2 \rightarrow CH_3 + CO$ | 4.83×10^{-04} | 4.0 | -2000.0 | $M + H_2O_2 \rightarrow 2OH + M$ | 1.30×10^{17} | 0.0 | 45500.0 |
| $C_2H_2 + O \rightarrow C_2H + OH$ | 3.16×10^{15} | -0.6 | 15000.0 | $H_2O_2 + H \rightarrow HO_2 + H_2$ | 1.60×10^{12} | 0.0 | 3800.0 |
| $CH_2CO + O \rightarrow CO_2 + CH_2$ | 1.75×10^{12} | 0.0 | 1350.0 | $H_2O_2 + OH \rightarrow H_2O + HO_2$ | 1.00×10^{13} | 0.0 | 1800.0 |
| $CH_2CO + H \rightarrow CH_3 + CO$ | 1.13×10^{13} | 0.0 | 3428.0 | $NO_2 + O \rightarrow NO + O_2$ | 1.00×10^{13} | 0.0 | 600.0 |
| $CH_2CO + H \rightarrow HCCO + H_2$ | 5.00×10^{13} | 0.0 | 8000.0 | $M + NO_2 \rightarrow NO + O$ | 1.10×10^{16} | 0.0 | 66000.0 |
| $CH_2CO + O \rightarrow HCCO + OH$ | 1.00×10^{13} | 0.0 | 8000.0 | $NH + O_2 \rightarrow HNO + O$ | 1.00×10^{13} | 0.0 | 12000.0 |
| $CH_2CO + OH \rightarrow HCCO + H_2O$ | 7.50×10^{12} | 0.0 | 2000.0 | $NH + O_2 \rightarrow NO + OH$ | 7.60×10^{10} | 0.0 | 1530.0 |
| $M + CH_2CO \rightarrow CH_2 + CO$ | 3.00×10^{14} | 0.0 | 70980.0 | $NH + NO \rightarrow N_2O + H$ | 2.40×10^{15} | -0.8 | 0.0 |
| $C_2H + O_2 \rightarrow 2CO + H$ | 5.00×10^{13} | 0.0 | 1500.0 | $H_2O + H \rightarrow H_2 + OH$ | 7.60×10^{13} | 0.0 | 15200.0 |
| $H + HCCO \rightarrow CH_2 + CO$ | 1.00×10^{14} | 0.0 | 0.0 | $M + N_2O \rightarrow N_2 + O$ | 1.62×10^{14} | 0.0 | 51600.0 |
| $O + HCCO \rightarrow 2CO + H$ | 1.00×10^{14} | 0.0 | 0.0 | $H_2O + O \rightarrow N_2 + O_2$ | 1.00×10^{14} | 0.0 | 28200.0 |
| $HCCO + O_2 \rightarrow 2CO + OH$ | 1.60×10^{12} | 0.0 | 854.0 | $H_2O + O \rightarrow 2HO$ | 1.00×10^{14} | 0.0 | 28200.0 |
| $CH + HCCO \rightarrow C_2H_2 + CO$ | 5.00×10^{13} | 0.0 | 0.0 | $H_2O + OH \rightarrow H_2 + HO_2$ | 2.00×10^{12} | 0.0 | 10000.0 |
| $2HCCO \rightarrow 2CO + C_2H_2$ | 1.00×10^{13} | 0.0 | 0.0 | $NH + OH \rightarrow HNO + H$ | 2.00×10^{13} | 0.0 | 0.0 |
| $C_2H + O \rightarrow CH + CO$ | 5.00×10^{13} | 0.0 | 0.0 | $NH + OH \rightarrow N + H_2O$ | 5.00×10^{11} | 0.5 | 28000.0 |
| $C_2H + OH \rightarrow HCCO + H$ | 2.00×10^{13} | 0.0 | 0.0 | $NH + N \rightarrow N_2 + H$ | 3.00×10^{13} | 0.0 | 0.0 |
| $2CH_2 \rightarrow C_2H_2 + H_2$ | 4.00×10^{13} | 0.0 | 0.0 | $NH + H \rightarrow N + H_2$ | 1.00×10^{14} | 0.0 | 0.0 |
| $CH_2 + HCCO \rightarrow C_2H_3 + CO$ | 3.00×10^{13} | 0.0 | 0.0 | $NH + O \rightarrow NO + H$ | 2.00×10^{13} | 0.0 | 0.0 |
| $C_3H_3 + O_2 \rightarrow CH_2CO + HCO$ | 3.00×10^{10} | 0.0 | 2868.0 | $M + HNO \rightarrow H + NO$ | 1.50×10^{16} | 0.0 | 48680.0 |
| $C_3H_3 + O \rightarrow CH_2O + C_2H$ | 2.00×10^{13} | 0.0 | 0.0 | H_2O 10.0, O_2 2.0, N_2 2.0, H_2 2.0 | | | |
| $C_2H_2 + O_2 \rightarrow HCCO + OH$ | 2.00×10^{08} | 1.5 | 30100.0 | $HNO + OH \rightarrow NO + H_2O$ | 3.60×10^{13} | 0.0 | 0.0 |
| $M + C_2H_2 \rightarrow C_2H + H$ | 4.20×10^{16} | 0.0 | 107000.0 | $HNO + H \rightarrow H_2 + NO$ | 5.00×10^{12} | 0.0 | 0.0 |
| $M + C_2H_2 \rightarrow C_2H_2 + H_2$ | 1.50×10^{15} | 0.0 | 55800.0 | $2HNO \rightarrow N_2O + H_2O$ | 3.95×10^{12} | 0.0 | 5000.0 |
| $M + C_2H_4 \rightarrow C_2H_3 + H$ | 1.40×10^{16} | 0.0 | 82360.0 | $HNO + NO \rightarrow N_2O + OH$ | 2.00×10^{12} | 0.0 | 26000.0 |
| $H_2 + O_2 \rightarrow 2OH$ | 1.70×10^{13} | 0.0 | 47780.0 | $N + NO \rightarrow N_2 + O$ | 3.27×10^{12} | 0.3 | 0.0 |
| $OH + H_2 \rightarrow H_2O + H$ | 1.17×10^{09} | 1.3 | 3626.0 | $N + O_2 \rightarrow NO + O$ | 6.40×10^{09} | 1.0 | 6280.0 |
| $O + OH \rightarrow O_2 + H$ | 4.00×10^{14} | -0.5 | 0.0 | $N + OH \rightarrow NO + H$ | 3.80×10^{13} | 0.0 | 0.0 |
| $O + H_2 \rightarrow OH + H$ | 5.06×10^{04} | 2.7 | 6290.0 | $HO_2 + NO \rightarrow NO_2 + OH$ | 2.11×10^{11} | 0.0 | -479.0 |
| $H + O_2 \rightarrow HO_2 + M$ | 3.61×10^{17} | -0.7 | 0.0 | $NO_2 + H \rightarrow NO + OH$ | 3.50×10^{14} | 0.0 | 1500.0 |
| H_2O 18.6, H_2 2.9, N_2 1.3 | | | | $2NH \rightarrow 2H + N_2$ | 7.20×10^{13} | 0.0 | 0.0 |

UNITS: A cm-mol/sec; B -; C cal/mol

LASER-INDUCED FLUORESCENCE MEASUREMENTS TO TEST CHEMICAL MECHANISMS OF PROMPT NO IN METHANE FLAMES

Dwayne E. Heard, Jay B. Jeffries, Gregory P. Smith and David R. Crosley
Molecular Physics Laboratory
SRI International
Menlo Park, CA 94025

ABSTRACT

Laser-induced fluorescence measurements have been made of the OH, CH and NO radicals in slightly rich methane/air flames burning at 30, 70 and 120 Torr; in the 30 Torr flame atomic hydrogen is also measured. Absolute NO and OH concentrations were determined using separate calibration experiments. Temperature profiles were deduced from OH rotational excitation scans, and fluorescence quenching rates for NO and CH were determined. Predicted profiles of the concentrations of these radical species as a function of height above the burner were obtained from a computer model of the flame, and comparison made with experiment. Good agreement is achieved for the relative concentration profiles, the absolute NO concentration, and concentration ratios between 30 and 70 Torr, although slight disagreement with the CH profile indicates there remain some unknown aspects of the flame chemistry.

INTRODUCTION

Although natural gas is a clean burning fuel, containing virtually no fuel-bound nitrogen or sulfur, its combustion in air forms NO_x pollutants. These emissions limit its use, and the degree of regulation is expected to become more stringent in the future. Thus reduction of NO_x emissions in practical natural gas systems is an important objective. A major part of attaining that goal is the development of a predictive computer model of the pertinent chemistry, validated by sensitive laboratory experiments.

At temperatures below 2000 K, the major method of NO production in hydrocarbon/air flames is by the prompt-NO route, especially for slightly fuel-rich conditions. This dominates in practical natural gas/air flames, which usually operate at temperatures below 2000 K. Even though average fuel/oxygen ratios may be on the lean side, there are always locally fuel-rich regions in a nonpremixed flame, which includes most practical burners.

The prompt NO mechanism, whose reactions occur near the flame zone, is largely that first postulated by Fenimore¹ in 1971. Much of this reaction mechanism has recently been extensively reviewed and discussed by Miller and Bowman.² The primary initiation reaction is that of the radical CH with the air nitrogen to produce HCN and nitrogen atoms. The HCN undergoes several oxidation steps to produce more N atoms; these atoms then react with OH and O₂ to form NO. Some of the NO can be back-converted to HCN through a series of reactions also involving CH radicals.

Much but not all of this chemistry is well understood. Because the desired level of prompt NO produced in natural/gas air flames is often tens of parts per millions, the reactive species responsible are also present at low concentrations. Accordingly, any sensitive test of the model predictions must involve measurements of these pertinent radical species with a high degree of spatial resolution. We have made laser-induced fluorescence measurements of atomic hydrogen and the free radicals CH, OH and NO in low pressure methane/air flames. The flame studied most extensively was burned at 30 Torr. A computer model of the flame chemistry was used to predict species profiles, and comparisons with experiment were made to identify key aspects of the prompt NO chemical mechanism.

EXPERIMENTAL DETAILS

The flames were supported on a 6 cm diameter porous plug McKenna burner, inside an evacuable chamber suitable for optical probing, described in more detail in Refs. 3 & 4. A shroud of Ar was employed to match the flame velocity at the burner surface and improve flame stability. The flame most extensively studied was slightly rich, with an equivalence ratio of 1.13, and at a pressure of 30 Torr. The high pressure flames were operated at the same equivalence ratio and same total flow rates, so they are positioned much closer to the burner surface. The flow rate was kept constant at all times for all flames studied in this work. All measurements were made using laser-induced fluorescence (LIF); the optical configuration remained the same whilst the burner was translated vertically with a minimum step size of 6 μm . Profiles as a function of height above the surface were typically measured with 125 μm between points and a spatial resolution between 0.2 mm and 1.0 mm.

Following laser excitation the fluorescence was collected at right angles and imaged onto a monochromator with attached photomultiplier (PMT), except in the case of H atoms, for which an interference filter centered at 656 nm was employed. The PMT signal was captured by a boxcar (SRS 250) and stored on computer through a CAMAC crate. Fluorescence lifetimes were measured using a Transiac 2001S 100 MHz digitizer. The laser energy was recorded in order to normalize the LIF signal on a shot-to-shot basis.

Collisions with the ambient flame gases quench the electronically excited states of the radicals, decreasing the fluorescence decay time from that given by the purely radiative rate. In the case of OH, the influence of quenching on the fluorescence quantum yield is avoided by the use of a short (20 ns duration) gate triggered promptly after the exciting laser pulse.⁵ For NO and CH, the lower signal levels require integration over a large fraction of the decay pulse, and quenching must be accounted for to determine relative concentration profiles. In the case of NO, the decay time in the flame is also needed to calibrate the absolute concentration by comparison with LIF from a known room temperature concentration.

Decay measurements were made in the 30 and 70 Torr flames for both NO and CH, using the transient digitizer, with 10 ns resolution. The details are reported elsewhere,⁶ where the experimental results for the 30 Torr flame are compared to those expected from current knowledge of species—specific cross sections for quenching of $A^2\Sigma^+ \text{NO}$ and $A^2\Delta \text{CH}$, together with a calculated composition of the flame. The agreement is good, within 20 to 30%. For both CH and NO, total quenching rate and thus fluorescence quantum yield were found⁶ to be independent of flame position within experimental errors of 10%.

TEMPERATURE MEASUREMENTS

Accurate temperature determinations are crucial to any meaningful comparison between measured and calculated species profiles. This is because of the highly nonlinear dependence of reaction rates on temperature; it is especially true in the case of prompt NO formation, owing to the considerable temperature dependence for reactions including $\text{CH} + \text{N}_2$. As discussed below, a systematic error of 40 K through the flame (about 2.5%, and the same as our random error bars) would alter the predicted NO concentration by nearly 25%.

The temperature profiles are also needed to reduce measured LIF intensities to ground state radical concentrations, accounting for the variation of the fraction of the molecules populating the absorbing level as a function of temperature. Accuracy is especially important for this purpose at the lower temperatures close to the burner surface.

LIF temperature measurements are made using rotational excitation scans in the (0,0) band of the OH radical, which provides strong signals throughout the flame. The special care that must be taken to avoid systematic errors in these measurements has been discussed.⁷ These include:

(1) use of a prompt detection gate, here 20 ns, to avoid problems caused by temperature and

rotational-level dependent quenching and radiative rates; (2) use of a detector with a uniform response over a wide bandpass, here 25 nm, to avoid biasing due to changes in the fluorescence spectrum with excited rotational level; (3) normalizing LIF signals by transmitted laser intensity to correct for non-zero optical depth; and (4) operating in a linear regime to avoid intensity anomalies due to satellites and line wings.

Temperatures were measured in the flame using a spectral fitting method. Fig. 1 shows how spectra taken at different heights above the burner surface vary with temperature. The top panel is near the peak, with a fitted temperature of 1672 K. The middle panel shows a spectrum at 1153 K, while the bottom panel exhibits the sparse spectrum found in the coolest region we could measure, 405 K at only 2.5 mm from the burner surface. Due to the near ambient temperature (achieved through water cooling) heterogeneous reactions at the burner surface are minimized.

The temperature profile in the 30 Torr flames is shown in the top left panel of Fig. 2. Temperature profiles were also measured in the 70 and 120 Torr flames, exhibiting a peak closer to the burner surface, but with approximately the same peak value. The error bars were larger in the higher pressure flames, and have been estimated at about 100 K. A smooth temperature profile was fitted to the data for each flame, and then used as input to the model as well as for analysis of the LIF intensity profiles to obtain species concentrations.

EXPERIMENTAL SPECIES PROFILES

OH--Most profiles were made using the $R_2(6)$ line of the (0,0) band of the A-X system; some checks using the $R_1(3)$ line showed excellent agreement after accounting for the difference in population fraction with temperature. The 20 ns duration, prompt gate avoided effects of quenching.⁵ The absolute OH concentration was measured at its peak value by an absorption measurement of 2% per cm for the $R_2(6)$ line and 1.5% per cm for $R_1(3)$, corresponding to a peak concentration of $(6 \pm 3) \times 10^{14}$ molecules/cm³, or a mole fraction of 0.0035 in the 30 Torr flame. Similar measurements at 70 Torr indicate approximately the same fractional peak concentration.

NO--The $Q_1(17)$ rotational line of the (0,0) band of the A-X system was used for the profiles, (again minimizing the temperature dependence of the absorption) while collecting the (0,2) fluorescence. The absolute NO concentration was obtained by calibration using LIF in known amounts of NO diluted in helium/argon mixtures, flowing through the burner at room temperature. The optical system was the same as in the flame; the ratio of the LIF signals under these conditions to those in the flame then furnished the desired calibration. In the room temperature flow, the decay is mainly radiative with a lifetime of 192 ns. The quenching rate in the 30 Torr flame at the peak of the NO signal is 2.9×10^7 s⁻¹. Taking the ratio of the two signals and the quenching and accounting for Boltzmann population difference of the absorbing rotational level yielded a peak NO concentration of $(7 \pm 4) \times 10^{11}$ molecules/cm³, or a fractional concentration of 4 ppm in the flame. From comparison of the relative LIF signals at 30 and 70 Torr, and applying the necessary quenching correction, a peak NO concentration of $1-3 \times 10^{12}$ molecules/cm³ was obtained at 70 Torr (3.2 ppm).

CH--Excitation and observation were performed in the (0,0) band of the A-X system. There was insufficient absorption to calibrate for an absolute CH concentration. However, the profiles taken at 30 and 70 Torr were used to obtain a ratio of the peak CH concentration at these two pressures, showing a decrease in CH concentration at 70 Torr, with the ratio $[\text{CH}]_{30 \text{ Torr}}/[\text{CH}]_{70 \text{ Torr}}$ being 1.7.

H Atoms--Hydrogen atoms were excited to the $n = 3$ level using two photons near 205 nm, with observation of the Balmer- α $n = 3 \rightarrow n = 2$ emission at 656 nm. In addition to LIF, amplified spontaneous emission (ASE) was also observed along the laser axis in both the forward and backward directions.

All intensity profiles were corrected to account for the Boltzmann fraction of the absorbing level at the local temperature. Profiles in the 30 Torr flame are given in Fig. 2 over a wide range of

measurement well into the burnt gases. For OH and NO, the absolute concentrations are given; for CH only a relative profile was obtained. The time decay measurements showed quenching of NO and CH to be invariant with position, so no quenching corrections were performed; the OH profiles were obtained with a prompt gate so they are not influenced by quenching. Also shown is the OH(A) chemiluminescence profile measured with the laser off, a result of the CH + O₂ reaction, which creates OH directly in the emitting A²Σ⁺ state.

At this point, it is useful to qualitatively describe the profiles of the three species in the 30 Torr flame. CH is sharply peaked at about 1.0 cm above the burner surface, similar to that of the chemiluminescence from OH(A), which is a direct product of the CH + O₂ reaction. The concentration of NO, OH, and H rise more slowly above the burner, and extend well past the flame front into the burnt gases. NO displays a bisigmoidal rise and this feature is discussed below. Profiles in the 70 and 120 Torr flames are not shown but are qualitatively similar, including a bisigmoidal NO profile at 70 Torr.

FLAME MODEL CALCULATIONS

A computer model of the chemistry of low pressure methane/air flames was assembled to compare predicted concentrations with the experimental profiles, and to gain some insight into the controlling kinetics. A basic mechanism was constructed, with rate constants of our choice⁸ based largely on the recommendations of Warnatz⁹ for hydrocarbon oxidation and of Miller and Bowman² for the prompt NO submechanism. This latter subset was selected according to the authors' flowcharts, and included deNO_x chemistry. A total of 148 reactions involving 38 species were included. Thermodynamic and transport input are from the Sandia databases,¹⁰ with slight modifications for the thermodynamics of the methylenes, formaldehyde, CH₂OH, and NCO.⁶ The OH(A) chemiluminescence is calculated according to production from the CH + O₂ reaction, and removal by collisional quenching on a time scale short compared to flow velocities or diffusion.

The flame model calculations were carried out using the Sandia flame code,¹¹ based on one dimensional fluid flow; it includes thermal diffusion, bimolecular and unimolecular kinetics, and sensitivity analysis for individual chemical reactions. Necessary inputs are the measured pressure and gas flow rates at the burner surface, and the measured temperature profile. Calculations were performed well out into the burnt gases, to a height of 10 cm above the burner for the 30 Torr flame. The cross-sectional area of the flame was assumed constant (see below). Predictions of the model are compared to experiment for order, peak position, width and shape of the species profiles, and the absolute concentrations. These comparisons form sensitive tests of our understanding of the flame chemistry.

SPECIES PROFILES

In Fig. 2, the computed concentrations have been matched to the maximum of the experimental values at 30 Torr. In relative position, the CH and OH(A) chemiluminescence reach their peaks at the half maximum point in the rise of ground state OH, i.e., at the flame front in both experiment and model. However, the predicted widths are slightly too small, by roughly a millimeter for CH, and the CH in the model rises a millimeter too late. This disagreement implies some errors in the chemistry controlling CH production and destruction, and thus entertains the expectation that the model will also be in error with respect to predicted NO production. Since the position of the OH rise is well predicted, it appears the overall oxidation chemistry is being modeled reasonably. The OH(A) chemiluminescence calculation appears to decay too rapidly, suggesting gaps in our mechanistic knowledge or a second production reaction.

The shapes of the NO and OH profiles are also adequately computed, although early OH is underpredicted, and the slight apparent decline of NO in the burnt gases is not calculated. The OH profile shows low but significant concentrations at early time (low height) due to diffusion. The rise and steepness of the OH are well predicted, within 1 mm, as is the decline in the burnt gases

via reaction with CO. The leveling off after 2 cm, the presence of NO at low heights, and the bisignoidality of the profile are well predicted by calculation. The match in absolute position of the NO rise is also good, although diffusion reduces the sharpness of the rise.

ABSOLUTE CONCENTRATIONS

Absolute concentration measurements form another sensitive test. The calculated peak OH concentration at 30 Torr is 50% above the measured value, just at the estimated confidence limit for the absorption measurement. The NO concentration calculated at 1.75 cm for the 30 Torr flame is 3.7 ppm compared to the measured, calibrated value of 4 ppm. This excellent agreement is surprising, given the uncertainty in the main rate constants to which NO is sensitive, in particular the controlling chemistry involving CH (see below).

Our choice of rate constant for the key $\text{CH} + \text{N}_2 \rightarrow \text{HCN} + \text{N}$ is based on the direct shock tube measurement of Dean et al.¹² A preliminary transition state theory extrapolation of these values to the lower temperatures of the flame indicates a simple Arrhenius expression is adequate. The value obtained from this rate constant expression is in substantial agreement at 1500 K with the value recommended by Miller and Bowman². An absolute measurement of the CH concentration was not performed in these experiments. The calculation predicts a peak mole fraction of only 2 ppm, very similar to that from another recent modeling study of a 0.1 atm methane/air flame.¹³

Model calculations were also made for the 70 Torr flame with the same stoichiometry and flow rates, using the measured temperature profile as input. The calculated mole fraction of NO formed is the same, in good agreement with the observed ratio of 0.8. The model also predicts a peak mole fraction of CH at 70 Torr of 35% of the 30 Torr value, which agrees excellently with the observed 0.25 ratio. This good agreement, although at present for a very limited set of conditions, offers encouragement for being able to predict pressure effects on prompt NO formation.

We briefly examined a few aspects of the kinetics associated with the profiles of NO, HCN, and NH. The early peak of NO is due to diffusion and its failure to react away at lower temperature. If we analyze all production rates for NO, there are no significant reactive sources in this region. The rise in NO early in the flame front occurs from the $\text{CH} + \text{N}_2$ reaction, which forms N atoms that are rapidly converted by oxygen to NO. Examination of reaction rates shows that almost all NO is from the prompt mechanism. The other product from the $\text{CH} + \text{N}_2$ reaction, HCN, also has a wide distribution showing that it has also diffused back to a nonreactive region, and that it takes longer to burn out. The NH distribution, which is the final step in the HCN oxidation process before N and NO production, occurs later in the calculated flame. These last steps are responsible for the final curvature in the profile near 2 cm. The peak NH concentrations are predicted to be in the 10 ppm range, and its LIF profile could be a useful diagnostic for this last portion of the prompt NO mechanism.

Sensitivity analysis indicates the $\text{CH} + \text{N}_2$ reaction to be the most important step in NO formation. Quantitative measurement and control of CH and its kinetics are clearly indicated as the key to reduction of NO_x emissions which result from prompt NO chemistry.

CONCLUSIONS

Laser-induced fluorescence measurements have been made of the species OH, CH and NO in a low-pressure methane/air flame and compared with predictions from a detailed computer model. Through measurement of several radicals, assessment of the goodness of the model does not rely on a single species comparison, and we can see which part of the model needs further investigation.

The model prediction of both the NO profile and its absolute concentration in this flame are in excellent agreement with experiments. A sensitivity analysis shows that the key reactions

controlling prompt NO are CH + N₂ plus those which control the CH concentration and position. However, the CH concentration profile is not in such good agreement with experiment.

The development of a measure of the predicted temperature sensitivity shows that this parameter, whose profile is taken as input to the model, is extremely important in NO prediction. Uncertainty in the temperature severely limits the ability to calculate or control the amount of prompt NO formed, even with perfect knowledge of kinetics. This could be particularly important for practical burners with nonpremixed flames where there exist a variety of temperature/concentration conditions.

The model also makes excellent predictions of the relative concentrations of both NO and CH as the pressure is raised from 30 Torr to 70 Torr. This suggests that the pressure dependence of the reaction rates is properly incorporated, and indicates that the model may be suitable for scaling to yet higher pressures. However, confirmation is needed at more than just this pair of pressures.

The success of the model is encouraging although there remain questions, especially concerning the ability to predict CH. Therefore we do not yet know the predictability of this reaction set, and need to make further measurements with different conditions (pressure and stoichiometry). Absolute measurement of the CH concentration would be a particularly useful addition to the results at hand, and a determination of NH would be valuable.

ACKNOWLEDGEMENT

We appreciate the support for this work, furnished by the Southern California Gas Company.

REFERENCES

1. C. P. Fenimore, Thirteenth Symposium (International) on Combustion, The Combustion Institute, Pittsburgh, 1971, p. 373.
2. J. A. Miller and C. T. Bowman, *Prog. Energy Comb. Sci.* **15**, 287 (1989).
3. K. J. Rensberger, M. J. Dyer, and R. A. Copeland, *Appl. Opt.* **27**, 3679 (1988).
4. M. J. Dyer, L. D. Pfefferle, and D. R. Crosley, *Appl. Opt.* **29**, 111 (1990).
5. K. Kohse-Höinghaus, J. B. Jeffries, R. A. Copeland, G. P. Smith, and D. R. Crosley, Twenty-Second Symposium (International) on Combustion, The Combustion Institute, Pittsburgh, 1988, p. 1857.
6. D. E. Heard, J. B. Jeffries, and D. R. Crosley, *Chem. Phys. Lett.*, in press (1991).
7. K. J. Rensberger, J. B. Jeffries, R. A. Copeland, K. Kohse-Höinghaus, M. L. Wise and D. R. Crosley, *Appl. Opt.* **28**, 3556 (1989).
8. G. P. Smith, *Combust. and Flame*, in preparation, 1991.
9. J. Warnatz, in *Combustion Chemistry*, W. G. Gardiner, Ed., (Springer-Verlag, N. Y., 1984).

10. R. J. Kee, F. M. Rupley, and J. A. Miller, Sandia National Laboratory Report SAND87-8215 (1987); R. J. Kee, J. Warnatz, and J. A. Miller, Sandia National Laboratory Report SAND83-8209 (1983).
11. R. J. Kee, J. F. Grcar, M. D. Smooke, and J. A. Miller, Sandia National Laboratory Report SAND85-8240 (1985).
12. A. J. Dean, R. K. Hanson, and C. T. Bowman, Twenty-Third Symposium (International) on Combustion, The Combustion Institute, Pittsburgh, 1991, in press.
13. M. C. Drake and R. J. Blint, Western States Meeting of the Combustion Institute, Paper 90-08, San Diego, Oct. 1990; General Motors Research Publication GMR-6922, 1990.

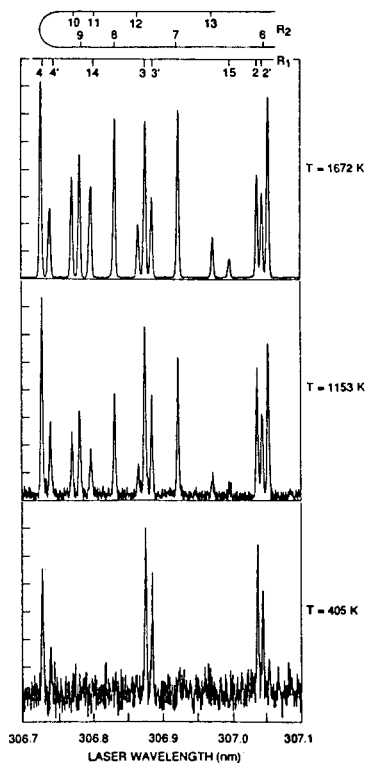


Figure 1 OH LIF rotational excitation spectra at three positions above the burner in the 30 Torr flame. Top: 3.22 cm height, 1672 K temperature; middle: 0.89 cm, 1153 K; bottom: 0.25 cm, 405 K.

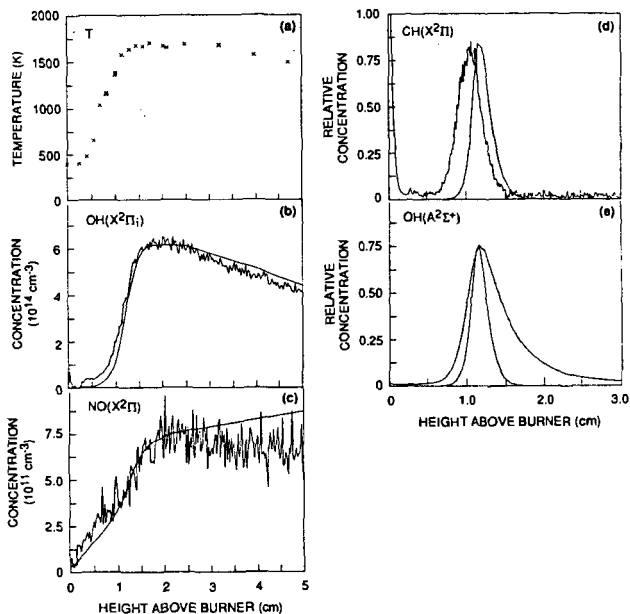


Figure 2 (a) Experimental temperature profile from OH LIF in the 30 Torr flame. A temperature of 399 K at the burner surface was assumed as a boundary condition for the flame model.

(b) - (e) Experimental and calculated species concentration profiles in the 30 Torr $\Phi = 1.13$ methane/air flame. Note the horizontal scale change for (d) CH(X²Π) and (e) OH(A²Σ⁺). Model profile species are given by the smooth lines, and the OH values have been scaled by a factor of 0.67 to match the peak experimental value. Scattered laser light from the burner surface can be seen in the CH profile (d).

LASER-INDUCED FLUORESCENCE DIAGNOSTICS AND MODELING OF 10 TORR METHANE/OXYGEN FLAMES

J.W. Fleming, K.A. Burton^a, and H.D. Ladouceur
Chemistry Division, Code 6110
Naval Research Laboratory, Washington, DC 20375-5000.

Keywords: methane, flame modeling, CH radical

^a NRC/NRL Postdoctoral Research Associate

ABSTRACT

Spatial concentration profiles for CH have been obtained using laser-induced fluorescence in several 10 torr CH₄/O₂ flames at equivalence ratios (Φ) between 0.8 and 1.3. The experimental flow rates, temperature profiles, and a published chemical mechanism have been used in Sandia's flame code to predict CH spatial positions. A comparison of experimental results and computer calculations are presented.

I. INTRODUCTION

The flame environment is one of the most interesting and complex chemical systems. Experimental efforts have been directed to identifying and quantifying molecular and atomic species in flames using a variety of techniques. An increasing experimental kinetics data base and computer modeling advances have made it possible to correlate experimental measurements with computer predictions. It is clear that experimentally monitoring all of the chemical species in any hydrocarbon combustion problem is impractical if not impossible. The ability to predict the behavior of most flame species based on a few experimental parameters is attractive and sometimes necessary for practical applications.

The flame zone is several millimeters wide at 10 torr which allows for the examination of CH with sufficient spatial resolution to resolve its growth and decay. This paper presents modeling and experimental comparisons for CH which extends our previous work.¹ The current work details the behavior of CH (experimental and predicted) for several 10 torr methane/oxygen flames of differing fuel equivalence ratios. We were particularly interested in the results for fuel-rich flames. We monitor OH radical distributions (for temperature measurements) and CH radical concentrations with laser-induced fluorescence, LIF.

II. EXPERIMENTAL

Measurements characterizing a steady-state 10 torr methane/oxygen flame have been outlined previously.¹ Experiments were carried out in a water-cooled, stainless steel 6-way cross containing a water-cooled flat-flame burner.² Pressure measurements were made at the top of the cross using MKS baratron heads. Pressures were maintained at 10 torr to within $\pm 0.5\%$. The flames are supported on a sintered bronze 6-cm diameter mantel. A shroud gas flow of Argon was used whose flow rate was adjusted to match the total mass flow through the burner for each flame studied. CH₄/O₂ flames were studied with equivalence ratios and flows listed in Table 1. The flow rates were measured with calibrated mass flow meters (Tylan). The methane and oxygen were premixed upstream from the burner. Total mass flow was maintained constant for all of the flames studied at 1.140 ± 0.005 mg/s-cm². The previously studied flame had a mass flow of 1.040 ± 0.005 mg/s-cm². Vertical translation of the burner via a bellows assembly with micrometer adjustment allowed a 10 cm range above the burner to be probed with a position reproducibility of ± 0.03 cm.

The CH and OH radicals were detected by LIF with the output of an excimer-pumped dye laser (Lambda Physik 101MSC/FL2002). The diameter of the probe beam was 0.8 mm. We measured CH intensity profiles as a function of position along the burner centerline by tuning the probe laser wavelength to the $P_1(6)$ transition in the $A^2\Delta - X^2\Pi(0,0)$ band at 431 nm (Coumarin 440 dye, Exciton). A Corion 4500 interference filter (433 nm center, 60 nm FWHM) allowed the collection of CH fluorescence in the (0,0) band. The probe laser energies were kept $\leq 4 \mu\text{J/pulse}$. There was essentially no scattered light in the CH experiments. Zeroes were obtained by tuning off of the peak. A second PMT monitored the probe laser intensity using scatter from a roughened aluminum plate. Gated integrators (SRS) monitored signals from the PMT's. The fluorescence signals were weighted by the temperature-dependent Boltzmann population of the probed level determined from the experimental temperature profile. The detected fluorescence signals were also corrected for obscuring of the LIF signal by the burner itself. We assumed a uniform CH electronic quenching rate throughout the flame which has been demonstrated to be reasonable in similar flames.^{3,4}

The flame temperature profiles were obtained using a Pt/ 13% Pt-Rh thermocouple (Omega - Type R, 0.01 inch diameter wire). The thermocouple leads were housed in a ceramic tube. The bare thermocouple was acid washed and then coated with a high temperature adhesive cement⁵ (Ceramabond 569) which was cured using the manufacture's recommended procedure. The coated junction was positioned above the center of the burner with the leads parallel to the burner surface. For OH temperature measurements, OH excitation spectra were obtained using the frequency doubled output of the dye laser (coumarin 540A, Exciton). The OH probe laser had a diameter ≤ 0.8 mm and the energy was kept below $0.5 \mu\text{J/pulse}$. OH radicals were excited in the $A^2\Sigma - X^2\Pi(1,0)$ band from 281 to 285 nm. A Corning 7-54 filter (320 nm center, 120 nm FWHM) transmitted fluorescence in the (1,0) and (0,0) band. Radiation corrections⁶ for the thermocouple readings were calibrated using the OH LIF rotational temperature measurements in the $\Phi = 0.9$ flame previously studied. The radiative effect of the burner surface to the thermocouple was accounted for by a view factor for a sphere to a disk.⁷

III. MODELING

We have previously shown that OH and CH relative concentration profiles could be reasonably modeled in a $\Phi = 0.9$ flame using the chemical mechanism of Miller and Bowman,⁸ excluding the nitrogen containing species. The same mechanism is used in this study and consists of 33 chemical species and 150 reversible reactions. Chemical thermodynamic data and rate coefficients were evaluated using CHEMKIN-II which can account for the pressure dependence of the appropriate reactions.

To model the CH profiles we used PREMIX,⁹ a one-dimensional flame code developed at Sandia for modeling premixed, laminar flames. PREMIX calculates the steady-state species spatial profiles and requires the following as input: a chemical mechanism, transport properties, total pressure, flow rate, burner diameter, and the vertical temperature profile.

IV. RESULTS AND DISCUSSION

A. Temperature measurements

Thermocouple measurements were made throughout each flame as a function of height above the burner. The thermocouple temperature readings were corrected as outlined above. Listed in Table 1 are the maximum corrected temperature reading for each flame. The corrected temperature profiles are shown in Figure 1. Typical corrections for the 0.15 cm diameter coated junction varied from 100 to 550 K over the measurement range of 1000 to 1700 K. These corrections are large but consistent with the large junction diameter used in these experiments. Such large diameters were necessary to insure the integrity of the coating. Uncoated thermocouple temperature measurements have been shown to be completely unusable in a similar flame due to the very large catalytic effect.¹ Flame

deposited SiO_2 coatings were found to be very fragile and could be used in only for a few measurements before the coating deteriorated. The Ceramabond coating was very sturdy, lasting for numerous flames, and is easy to apply.

Also presented in Figure 1 are the LIF OH rotational temperature measurements for the $\Phi = 0.8$ flame. The agreement is very good for this flame which has a 10% higher gas flows than the calibration flame. Temperatures at 1.5 cm above the burner for all of the flames were measured using OH excitation spectra as a check on the correction method used. Very good agreement was found for all of the flames at this position, the corrected reading always within the $\pm 2 \sigma$ experimental uncertainty.

B. Concentration measurements

Experimental relative concentration profiles for CH are shown in Figure 2 for flames $\Phi = 0.8, 0.9,$ and 1.0 . Results for flames $\Phi = 1.15$ and 1.3 are presented in Figure 3. Symbols in both of these figures are connected with a dashed line and the symbol legend is presented in Figure 1. All experimental concentrations are on the same relative scale (left axis). Also shown in Figures 2 and 3 with solid lines are the PREMIX calculated steady-state CH profiles (right axis) for the respective equivalence ratios. The two vertical axes (relative and absolute) have been chosen such that the maximum experimental concentration for $\Phi = 1.0$ flame equals the PREMIX calculated maximum for that flame.

The qualitative shape of these profiles were as expected. Ground state CH radicals peak in each of the flames and the distances of these peaks above the burner surface are found to increase with higher equivalence ratio. Such behavior has also been observed in 40 torr C_2H_2 flames.¹⁰ The general shape of the calculated CH steady-state profiles is in qualitative agreement with the experimental profiles. Higher CH concentrations are observed for higher flame equivalence ratios. Table 2 summarizes the quantitative comparison of the significant results: location of the profile maximum, the profile width, and concentration. The location of the profile maximum above the burner is reasonably well predicted for all of the flames. The model predicts the peak location to be approximately 1 mm closer to the burner than observed experimentally for each of the flames. This difference appears to be constant for all of the flames. For the profile widths, the calculated widths (FWHM) are the same as the experimentally observed widths within experimental uncertainty. For the concentration comparison, the calculated concentrations were divided by the relative experimental concentrations and then multiplied by the experimental profile for the $\Phi = 1.0$ flame. Table 2 shows that the $\Phi = 0.8, 0.9, 1.0,$ and 1.15 flames are in good agreement within experimental uncertainty assuming the above scaling method. The largest difference is the slight over prediction of the $\Phi = 1.3$ flame. This may be due to the presence of higher hydrocarbons in the richer system which are not in the chemical mechanism. Another assumption made is that the quenching rate is a constant as a function of height above the burner. Although this is valid for methane flames, it has been shown to break down in flames using higher hydrocarbon fuels.¹¹

CH concentration profiles are very sensitive to the spatial temperature profile. The very good agreement of the location of the concentration maxima between predicted and calculated and the good agreement for the $\Phi = 0.8$ flame between corrected thermocouple readings and LIF OH measurements, suggest that the thermocouple coating and correction method employed here is valid. The position of 1.5 cm above the burner for comparing the corrected thermocouple measurements with the OH rotational temperatures was chosen because of the fairly small temperature gradient at this position and the fairly good temperature separation of the flames (see Figure 1). A small systematic error in the temperature measurement in the region just above the burner is difficult to determine due to the very large temperature gradient present there and the finite probe size for both a thermocouple or a laser probe beam.

VI. CONCLUSIONS

The agreement between experimental measurements and modeling calculations of CH concentration profiles for 10 torr methane/oxygen flames has extended confidence in the predictive ability of the behavior of this specie in fuel-lean to slightly fuel-rich flames. These results indicate that the chemical mechanism used is consistent with the experimental observations but are not a confirmation of the mechanism or a verification of any individual kinetic rate. These results along with other species measurements, primarily other radical species, will begin to verify the chemical mechanism. Although CH is a minor chemical player in any hydrocarbon flame, the presence of ground-state CH only in the flame front makes the ability to predict its behavior extremely useful.

VII. ACKNOWLEDGEMENTS

We thank Robert Kee of Sandia National Laboratories for providing the PREMIX and CHEMKIN codes. We also acknowledge the Office of Naval Research for funding this research.

VIII. REFERENCES

1. Fleming, J.W.; Burton, K.A. and Ladouceur H.D., Chem. Phys. Lett. **175** (4), 395-400 (1990).
2. Low-pressure model flat-flame burner obtained from McKenna Products, Inc, Pittsburg, CA.
3. Cattolica, R.J.; Stepowski, D.; Puechberty, D. and Cottreau, M., J. Quant. Spectrosc. Radiat. Transfer, **32**, 363-370 (1984).
4. Rensberger, K.J.; Dyer, M.J. and Copland, R.A. Appl. Opt., **27**, 2768-2775 (1988).
5. Aremco Products, Inc., 23 Snowden Ave., Ossining, NY 10562.
6. Fristrom, R.M.; Westenberg, A.A., Flame Structure; McGraw-Hill, New York, 1965; pp 150-152.
7. Siegel, R.; Howell, J.R., Thermal Radiation Heat Transfer; McGraw-Hill, New York, 1981; p.830.
8. Miller, J.A. and Bowman, C.T., Prog. Energy Combust. Sci. **15**, 287-338 (1989).
9. "PREMIX: A Fortran Program for Modeling Steady Laminar One-Dimensional Premixed Flames," Kee, R.J.; Grcar, J.F.; Smooke, M.D. and Miller, J.A., Sandia Report SAND85-8240 (1987).
10. Joklik, R.G., Daily, J.W. and Pitz, W.J. Twenty-first Symposium (International) on Combustion, (The Combustion Institute, 1988) pp 895-904.
11. Rensberger, K.J.; Dyer, M.J. and Copland, R.A. Appl. Opt., **27**, 3679-3689 (1988).

Table 1. Experimental Conditions^{a,b}

| Φ | CH ₄ (slpm) | O ₂ (slpm) | Maximum T ^c (K) |
|--------|---------------------------|--------------------------|-------------------------------|
| 0.8 | 0.44 | 1.10 | 2006 |
| 0.9 | 0.67 | 1.08 | 2093 |
| 1.0 | 0.53 | 1.06 | 2169 |
| 1.15 | 0.59 | 1.03 | 2273 |
| 1.3 | 0.65 | 1.00 | 2286 |

^a Total mass flows for each of the flames was 1.140 ± 0.005 mg/s/cm².

^b Argon shroud gas was flowed to match the mass flow rate in the burner.

^c Radiation corrected temperature (see text).

Table 2. Comparison of Experimental and Modeling Results

| Flame Φ | Profile Maximum Location (cm) | | | Profile Width (cm) | | Peak Height Ratio Model/Experiment (Scaled to $\Phi = 1.0$) ^c |
|-----------------|----------------------------------|-------|-----------------------------|-------------------------|-------|---|
| | Experiment ^a | Model | Difference (Exp - Model) | Experiment ^b | Model | |
| 0.8 | 0.55 | 0.49 | 0.06 | 0.80 | 0.64 | 0.79 ± 0.19 |
| 0.9 | 0.60 | 0.51 | 0.09 | 0.71 | 0.68 | 1.07 ± 0.21 |
| 1.0 | 0.65 | 0.55 | 0.10 | 0.75 | 0.72 | 1.00 |
| 1.15 | 0.75 | 0.66 | 0.09 | 0.86 | 0.78 | 1.27 ± 0.22 |
| 1.3 | 0.95 | 0.84 | 0.11 | 1.03 | 0.93 | 1.72 ± 0.29 |

^a ± 0.08 cm uncertainty includes the measured positional uncertainty and the laser probe radius.

^b ± 0.16 cm uncertainty.

^c $\pm 2 \sigma$.

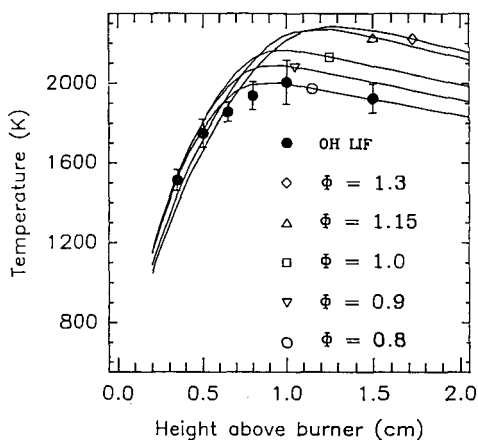


Figure 1. Temperature measurements as a function of height above the burner for the flame listed in Table 1: Corrected readings for a coated Pt/Pt-13% Rh thermocouple (solid lines); OH LIF temperatures derived from excitation spectra (filled circles) for the $\phi = 0.8$ flame.

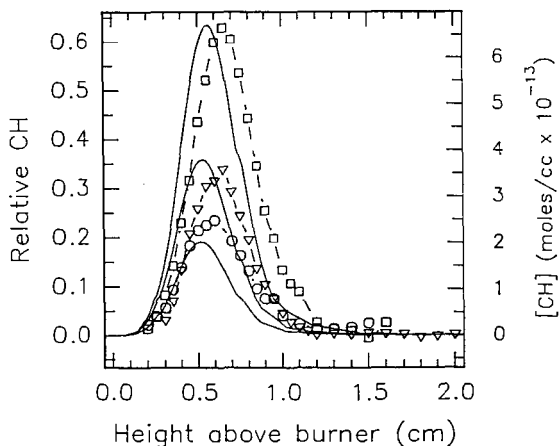


Figure 2. Concentration profiles for CH versus height above the burner for the flames $\phi = 0.8, 0.9, 1.0$, listed in Table 1 (symbol legend defined in Figure 1): Experimental concentration profile (symbols connected with a dashed line, left axis); PREMIX calculated CH radical profile using chemical mechanism listed in Reference 8 (solid line, right axis). Relative experimental concentrations have been scaled to the PREMIX calculated maximum value for the $\phi = 1.0$ flame.

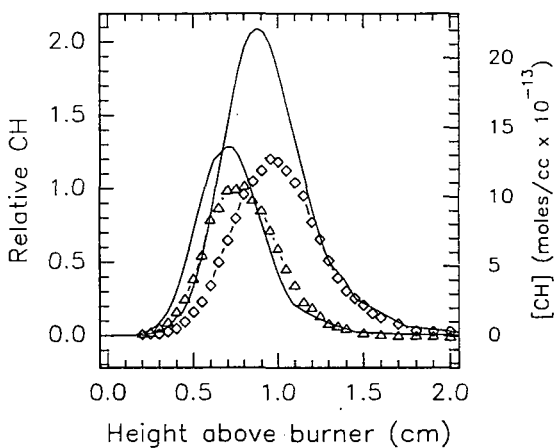


Figure 3. Concentration profiles for CH versus height above the burner for flames $\Phi = 1.15$ and 1.3 , listed in Table 1 (symbol legend defined in Figure 1): Experimental concentration profile (symbols connected with a dashed line, left axis); PREMIX calculated CH radical profile using chemical mechanism listed in Reference 8 (solid line, right axis). Relative experimental concentrations have been scaled to the PREMIX calculated maximum value for the $\Phi = 1.0$ flame.